

Chapter 2

Nonlinear Vibration Phenomena

Abstract Nonlinear systems have a range of behaviour not seen in linear vibrating systems. In this chapter the phenomena associated with nonlinear vibrating systems are described in detail. In the absence of exact solutions, the analysis of nonlinear systems is usually undertaken using approximate analysis, numerical simulations and geometrical techniques. This form of analysis has become known as *dynamical systems theory* (or sometimes *chaos theory*) and is based on using a system *state space*. In this chapter the basic ideas of dynamical systems are applied to vibrating systems. Finally, the changes in system behaviour as one (or more) of the parameters is varied are discussed. Such changes are known as *bifurcations*, and they are highly significant for the understanding of nonlinear systems.

2.1 State Space Analysis of Dynamical Systems

In this chapter only continuous time *deterministic* dynamical systems are considered. This means that, even if the system output looks very complicated, it is entirely determined by the input with no random effects. The state of the system is measured by the state vector, $\mathbf{x} = \{x_1, x_2, \dots, x_n\}^T$. The x_i are variable quantities such as positions and velocities, which describe what ‘state’ the system is in at any point in time, t . In a dynamical system, the states vary with time; so each state is a function of time, which for the i th state is written as $x_i(t)$. The states are sometimes referred to as the *dependent* variables, in that they depend on (are a function of) t . Time, t is then referred to as the *independent* variable, meaning that it is not a function of anything else.

The state vector has n states, often written as $\mathbf{x} \in \mathbb{R}^n$, which means that \mathbf{x} can be plotted in an n -dimensional Euclidean space.¹ This is called the *state space* or sometimes the *phase space* of the system. When $n > 3$ the state space cannot be plotted directly, but instead *projections* of \mathbf{x} are plotted, usually in either two or three dimensions. A plot of representative solutions (or trajectories) in phase space

¹ Think of \mathbb{R} as representing the set of real numbers on an axis in an n -dimensional space.

is called a *phase portrait*, and an important special case is a two-dimensional plot of displacement against velocity.

A dynamical system is one where the state of the system evolves over time. It is assumed that this evolution is governed by a differential equation which can be written in a general form as

$$\frac{d\mathbf{x}}{dt} = \mathbf{f}(\mathbf{x}, t). \quad (2.1)$$

Here \mathbf{x} is the vector representing the state of the systems at any time, t , and $\mathbf{f}(\mathbf{x}, t)$ is a vector of nonlinear functions governing the time evolution of the system.² If \mathbf{f} has no dependence on time, $\mathbf{f} = \mathbf{f}(\mathbf{x})$, the system is said to be autonomous, when $\mathbf{f} = \mathbf{f}(\mathbf{x}, t)$ is a function of time, the system is called non-autonomous.³ Equation (2.1) is often written as

$$\dot{\mathbf{x}} = \mathbf{f}(\mathbf{x}, t),$$

where an overdot represents differentiation with respect to time, t , and the state vector $\mathbf{x} = \{x_1, x_2, \dots, x_n\}^T$.

2.1.1 Harmonically Forced Linear Oscillator

First consider how this framework would work for the harmonically forced (and so non-autonomous) linear oscillator (Eq. (1.16) with $F_e = F_0 \cos(\Omega t)$)

$$\ddot{x} + 2\zeta\omega_n\dot{x} + \omega_n^2x = \frac{F_0}{m} \cos(\Omega t), \quad (2.2)$$

where ζ is the damping ratio and ω_n is the natural frequency. Define the state vector $\mathbf{x} = \{x_1, x_2\}^T$, where $x_1 = x$ is the displacement and $x_2 = \dot{x}$ is the velocity. Using these definitions notice that $\dot{x}_1 = x_2 = \dot{x}$, and $\dot{x}_2 = \ddot{x}$ which enables the system to be written in first-order form. This means there are no terms differentiated more than once. In general, all linear systems can be reduced to this form, and in this case the first-order form gives

$$\begin{aligned} \dot{x}_1 &= x_2 \\ \dot{x}_2 &= -2\zeta\omega_n x_2 - \omega_n^2 x_1 + \frac{F_0}{m} \cos(\Omega t), \end{aligned}$$

or

² Throughout, it will be assumed that \mathbf{f} is a smooth function, such that existence and uniqueness of solutions is always satisfied.

³ For most vibration problems, non-autonomous means the system has time-dependent forcing, and autonomous means that the system is unforced. In fact, a non-autonomous system can usually be represented as autonomous by setting $t = x_3$ and adding an additional equation to the system $\dot{x}_3 = 1$.

$$\begin{bmatrix} \dot{x}_1 \\ \dot{x}_2 \end{bmatrix} = \begin{bmatrix} 0 & 1 \\ -\omega_n^2 & -2\zeta\omega_n \end{bmatrix} \begin{bmatrix} x_1 \\ x_2 \end{bmatrix} + \begin{bmatrix} 0 \\ \frac{F_0}{m} \cos(\Omega t) \end{bmatrix},$$

which can be written in matrix notation as

$$\dot{\mathbf{x}} = \mathbf{A}\mathbf{x} + \mathbf{F}(t), \quad (2.3)$$

where \mathbf{A} is a constant matrix and $\mathbf{F}(t)$ is a vector of forcing terms. If the system is unforced (autonomous), then $\mathbf{F} = 0$ so that $\dot{\mathbf{x}} = \mathbf{A}\mathbf{x}$. This is the standard form for a linear dynamical system. It can be said that Eq. (2.3) is in ‘state space form’.

Example 2.1 Steady-state solutions for a harmonic oscillator

Problem Find the steady-state behaviour of the example for the harmonic oscillator defined by Eq. (2.2), when the mass $m = 1$ kg, natural frequency $\omega_n = 1$ rad/s, forcing frequency $\Omega = 1$ rad/s, forcing amplitude $F_0 = 10$ N and damping ratios $\zeta = 0.0625, 0.125, 0.25$. Plot the steady-state solution results for the three different damping cases in a two-dimensional graph of displacement against velocity.

Solution For three different values of damping ratio, $\zeta = 0.0625, 0.125, 0.25$, the steady-state solutions can be computed using 4th order Runge-Kutta numerical integration,⁴ to compute time series from initial values (see for example Fausett (1999)). The results are plotted in Fig. 2.1 which is a two-dimensional plot of displacement (x_1) against velocity (x_2). It can be seen that, in this case, the system behaviour is to form a circular orbit (if $\omega_n \neq 1$ the orbits will be elliptical) for each damping value. This steady-state behaviour is like simple harmonic motion, except with the addition of damping and forcing. The size of each ellipse is directly related to the balance of energy between the forcing input and the energy dissipated by damping. As the damping increases, the size of the ellipse reduces because more energy is dissipated by the viscous damper. This type of steady-state orbit is called a *limit cycle*, which is discussed in more detail in Sect. 2.5. ■

Now consider the more general case of a state space solution curve for a nonlinear system. An example of 20 s of data is shown in Fig. 2.2, as a solid black line with a start point in the plane $t = 0$ s and finishing in the plane $t = 20$ s. Three *projections* of this three-dimensional solution curve are also shown in Fig. 2.2. The displacement versus time plot is the projection onto the (t, x_1) plane and the velocity versus time plot is the projection onto the (t, x_2) plane. The projection onto the (x_1, x_2) plane is called the *phase portrait*, and is used extensively as a way of analysing the dynamics of the second-order nonlinear oscillators—the example shown in Fig. 2.2 is from a forced Duffing oscillator.

Individual solutions curves, such as the one shown in Fig. 2.2 are called either *trajectories* or *orbits*. The time evolution of multiple nearby trajectories is called the *flow* of a dynamical system—see Guckenheimer and Holmes (1983) for a more detailed discussion.

⁴ Although this linear system can be solved exactly, numerical integration is used as this will be required for the nonlinear examples.

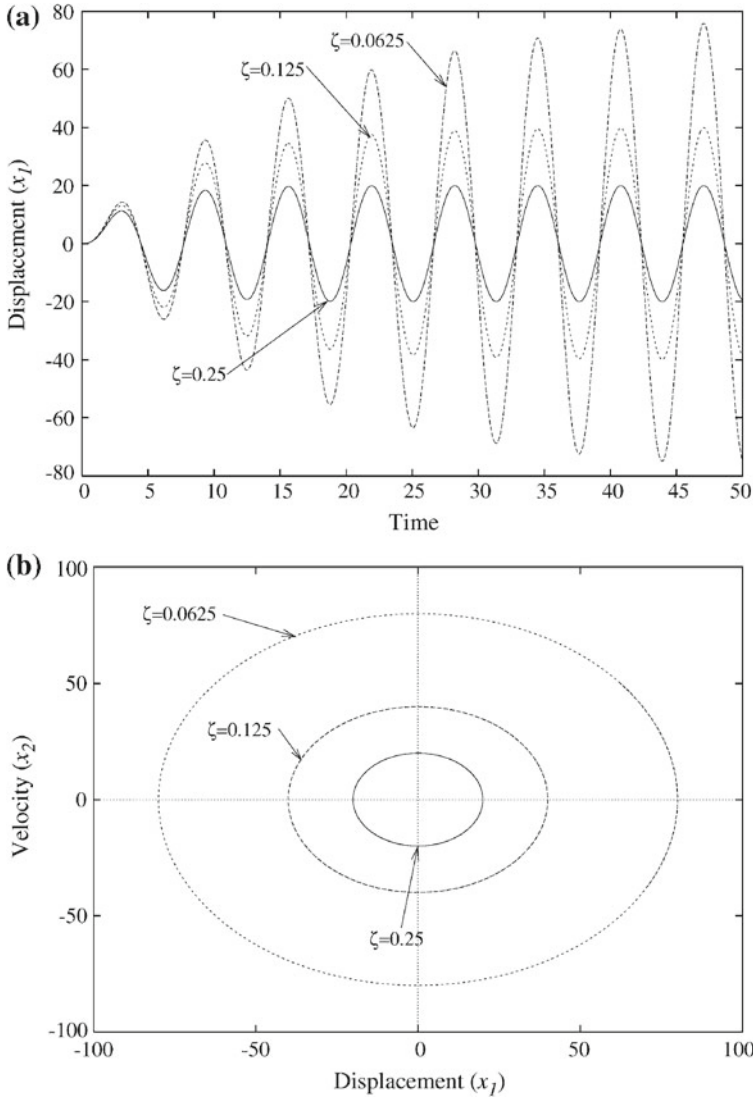


Fig. 2.1 Numerically computed solutions for a harmonic oscillator, **a** time series, and **b** steady-state periodic solutions

2.1.2 Equilibrium Points

When $\mathbf{f}(\mathbf{x}, t) = 0$ the system is said to have a *stationary point* or *equilibrium point*.⁵ Equilibrium points will be denoted as \mathbf{x}^* , so that $\mathbf{f}(\mathbf{x}^*, t) = 0$.

⁵ These are also sometimes called *fixed points* but here fixed point will only be used for maps.

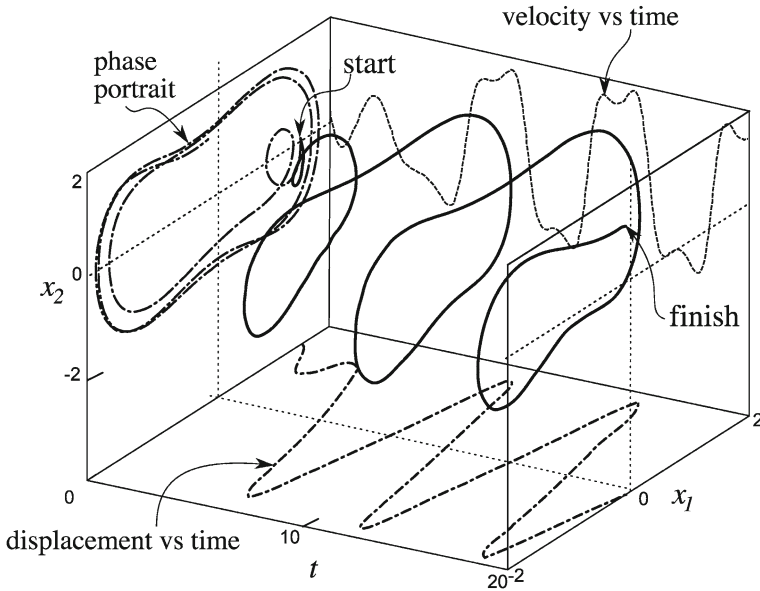


Fig. 2.2 State space for a forced Duffing oscillator

Equilibrium points play an important role in the analysis of nonlinear systems. This is because the dynamic behaviour close to an equilibrium point can normally be studied using a localized linear analysis. As a result, the study of a nonlinear system usually begins with identifying the equilibrium points. For simple systems, like the majority of those discussed in this book, the equilibrium points can be found by inspection of the state equations, Eqs. (2.1) and (2.2). In more complex systems, a Newton algorithm, or equivalent numerical technique, can be used to find solutions to $\mathbf{f}(\mathbf{x}, t) = 0$.

For harmonically forced nonlinear oscillators, the equation of motion can be rewritten as

$$\frac{d\mathbf{x}}{dt} = \mathbf{f}(\mathbf{x}) + \mathbf{F}(t), \quad (2.4)$$

where $\mathbf{F}(t)$ is the harmonic forcing vector, and the nonlinear function is autonomous. Then the analysis of the system equilibrium points can be simplified by first considering the unforced case when $\mathbf{F} = 0$. Here is an example.

Example 2.2 Equilibrium points and phase portrait for undamped pendulum oscillations

Problem Find the equilibrium points and draw the phase portrait for the undamped pendulum (introduced in Chap. 1) shown schematically in Fig. 1.5a, where the mass is assumed to act at a single point supported by a massless inextensible rod of length l .

Solution If no damping is assumed, the equation governing the motion of the pendulum is

$$\ddot{\theta} + \omega^2 \sin \theta = 0, \quad (2.5)$$

where θ is the angle from the downward equilibrium position, $\omega^2 = g/l$ rad/s, l is the length of the pendulum (of mass m) and g is the acceleration due to gravity (m/s²) (see Sect. 1.2.2 for a physical explanation of how this equation is derived). The state of the pendulum at any time t is uniquely defined by its position (angle) and velocity (angular velocity). So, to define the state vector, let $x_1 = \theta$ and $x_2 = \dot{\theta}$ then $\dot{x}_1 = x_2$ and substitute these relationships into Eq. (2.5), $\dot{x}_2 = -\omega^2 \sin(x_1)$. So the system can be written in the first-order form

$$\begin{bmatrix} \dot{x}_1 \\ \dot{x}_2 \end{bmatrix} = \begin{bmatrix} x_2 \\ -\omega^2 \sin(x_1) \end{bmatrix},$$

which is an autonomous first-order system of the form $\dot{\mathbf{x}} = \mathbf{f}(\mathbf{x})$.

The equilibrium points occur when $\mathbf{f}(\mathbf{x}) = 0$. For $\mathbf{f}(\mathbf{x}) = 0$ to occur, x_2 must be zero and x_1 must be either zero or $\pm n\pi$, where $n = 1, 2, 3 \dots$ because the sine function is zero at integer multiples of π . The case where $x_1 = 0$ corresponds to $\theta = 0$ which is the downward resting position—see Fig. 1.5a. If the pendulum rotates by 360° (2π rad) then it is back at the downward resting position, which is the case for all even n . When $x_1 = \pi$ the pendulum is in the upward position, which is unstable (like trying to balance a pencil on your finger tip), so that just the smallest disturbance will destabilize the equilibrium position.⁶

For the case when $x_1 - x^*$ is small, it is possible to examine the dynamic behaviour of the system close to the equilibrium points. For the x_1 equilibrium point, when x_1 is small, the approximation $\sin(x_1) \approx x_1$ can be made so that

$$\begin{bmatrix} \dot{x}_1 \\ \dot{x}_2 \end{bmatrix} \approx \begin{bmatrix} x_2 \\ -\omega^2 x_1 \end{bmatrix}. \quad (2.6)$$

This equation approximates the dynamics of the system close to the origin, where there is an equilibrium point $(x_1, x_2) = (0, 0)$, and additional equilibrium points for even values of n . To eliminate time, and observe the behaviour in the displacement versus velocity plane, take the ratio of the two velocity expressions in Eq. (2.6) to give

$$\frac{\dot{x}_2}{\dot{x}_1} = \frac{dx_2/dt}{dx_1/dt} = \frac{dx_2}{dx_1} = \frac{-\omega^2 x_1}{x_2}. \quad (2.7)$$

Equation (2.7) can be rearranged to give $-\omega^2 x_1 dx_1 = x_2 dx_2$, which can then be integrated. By incorporating the 1/2 factors into the constant of integration, the following

⁶ An interesting nonlinear control problem is to stabilize a pendulum in the upright (or inverted) position—see, for example the discussion in Sontag (1998) and Chap. 3.

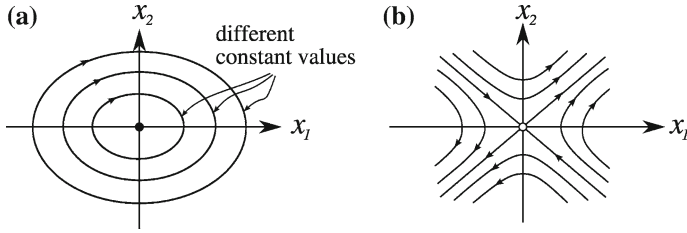


Fig. 2.3 Local equilibrium point dynamics: **a** centre, **b** saddle, *arrows on the flow lines indicate increasing time*

expression are obtained⁷

$$-\omega^2 x_1^2 = x_2^2 - \text{const} \rightsquigarrow x_2^2 + \omega^2 x_1^2 = \text{const}.$$

This is the equation of an ellipse that goes around the equilibrium point. The size of the ellipse depends on the constant (const), and as the constant is arbitrary, multiple ellipses exist close to the equilibrium point, as shown in Fig. 2.3a. This type of equilibrium point is known as a *centre*.

To study what happens close to the second equilibrium point, $(x_1, x_2) = (\pi, 0)$ when the pendulum is in the upward position, the x_1 coordinate needs to be shifted from zero to π , so that the sine term becomes

$$\begin{aligned} \sin(x_1 + \pi) &= \sin(x_1) \cos(\pi) + \cos(x_1) \sin(\pi), \\ &= \sin(x_1)(-1) + 0 = -\sin(x_1). \end{aligned}$$

So in this case the linearized equation becomes

$$\begin{bmatrix} \dot{x}_1 \\ \dot{x}_2 \end{bmatrix} \approx \begin{bmatrix} x_2 \\ \omega^2 x_1 \end{bmatrix},$$

and dividing \dot{x}_2 by \dot{x}_1 gives

$$\frac{\dot{x}_2}{\dot{x}_1} = \frac{dx_2/dt}{dx_1/dt} = \frac{\omega^2 x_1}{x_2} = \frac{dx_2}{dx_1}. \quad (2.8)$$

Equation (2.8) can be rearranged to give $\omega^2 x_1 dx_1 = x_2 dx_2$, which can then be integrated and, as before, by incorporating the 1/2 factors into the constant of integration, we can obtain the following expression

$$\omega^2 x_1^2 = x_2^2 - \text{const} \rightsquigarrow x_2^2 - \omega^2 x_1^2 = \text{const},$$

⁷ Note that this is now the same as the equation of motion for an unforced, undamped, harmonic oscillator, where the constant is determined by the initial displacement and velocity.

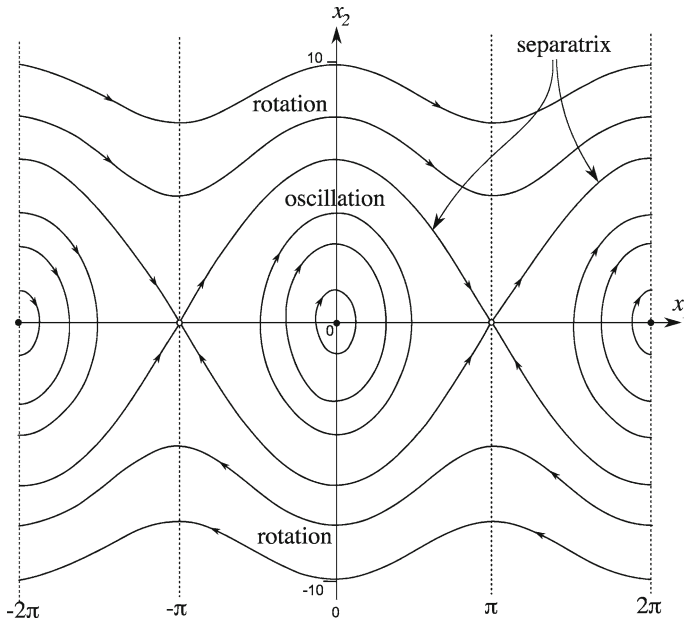


Fig. 2.4 Phase portrait for the undamped pendulum

which is the equation for a hyperbola, as shown in Fig. 2.3b. This type of equilibrium point is known as a *saddle*.⁸

Away from the equilibrium points the solution curves are governed by

$$\frac{dx_2}{dx_1} = \frac{-\omega^2 \sin(x_1)}{x_2},$$

from which

$$\int x_2 dx_2 = \int \omega^2 \sin(x_1) dx_1 \rightsquigarrow \frac{x_2^2}{2} = \omega^2 \cos(x_1) + \text{const},$$

so that the relation governing the phase portrait trajectories is

$$x_2 = \pm \sqrt{2(\omega^2 \cos(x_1) + \text{const})}.$$

Using this relationship we can draw the complete phase portrait. An example is shown in Fig. 2.4. ■

Notice that the equilibrium points are shown as solid black dots in the stable case (pendulum down) and as an unfilled circle to represent the unstable case (pendulum

⁸ In three dimensions this point looks like a horse saddle. See Sect. 2.3.

balanced upright). In Fig. 2.4 only a section of the phase portrait is shown from $-2\pi \leq x_1 \leq 2\pi$. The space continues in both directions with exactly the same pattern of alternating saddles and centres. The orbit which goes through the saddle point is called the *separatrix*⁹ because it separates two different types of behaviour. On the inside of the separatrix, oscillations occur around the stable centre point, which corresponds to constant values of $0 < \text{const} < \omega^2$. Outside the separatrix, the solution curves travel continuously to the right (above) or to the left (below), which corresponds to $\text{const} > \omega^2$. Physically, this corresponds to the pendulum rotating continuously with either positive angle (to the right) or negative angle (to the left). On the separatrix $\text{const} = \omega^2$.

2.1.3 Local Linear Approximation Near Equilibrium Points

Close to the equilibrium points the nonlinear system can be *linearized*. This is done by first changing coordinates to make the equilibrium point the origin of a new coordinate system. Defining a new coordinate vector $\xi = x(t) - x^*$, means that $\xi = 0$ corresponds to the equilibrium point of interest. If \mathbf{f} is autonomous (i.e. a function of x and not t) then

$$\frac{d\xi}{dt} = \frac{dx}{dt} = \mathbf{f}(x) = \mathbf{f}(x^* + \xi),$$

such that the dynamical system in terms of the new coordinates becomes

$$\frac{d\xi}{dt} = \mathbf{f}(x^* + \xi). \quad (2.9)$$

This is because x^* is a constant so $\dot{\xi} = \dot{x}$. To find the linearized system, $\mathbf{f}(x^* + \xi)$ is expanded as a Taylor series expansion

$$\mathbf{f}(x^* + \xi) = \mathbf{f}(x^*) + D_{x^*}\mathbf{f} \xi + \mathcal{O}(\|\xi\|^2), \quad (2.10)$$

where $D_{x^*}\mathbf{f}$ is the *Jacobian matrix* evaluated at x^* and $\mathcal{O}(\|\xi\|^2)$ denotes terms of second-order and higher.¹⁰ The Jacobian gives the linear gradients of the nonlinear function, \mathbf{f} , with respect to the states x_1 and x_2 .

For an equilibrium point, $\mathbf{f}(x^*) = 0$ by definition, so Eq. (2.10) becomes

$$\mathbf{f}(x^* + \xi) = D_{x^*}\mathbf{f} \xi + \mathcal{O}(\|\xi\|^2). \quad (2.11)$$

⁹ Also known as a heteroclinic orbit, which joins two separate saddle points. Not to be confused with a homoclinic orbit, an orbit which starts and finishes at the same saddle point.

¹⁰ Note that the norm is used here because ξ is a vector.

Both Eqs. (2.10) and (2.11) indicate that terms of second-order and higher-orders are ignored. If ξ is small, i.e. $\|\xi\| \ll 1$, then this type of assumption can be justified,¹¹ but it means that the analysis is valid only in a small region close to the equilibrium point.

In general, the Jacobian matrix is given by

$$D_{\mathbf{x}}\mathbf{f} = \begin{bmatrix} \frac{\partial f_1}{\partial x_1} & \frac{\partial f_1}{\partial x_2} & \cdots & \frac{\partial f_1}{\partial x_n} \\ \frac{\partial f_2}{\partial x_1} & \frac{\partial f_2}{\partial x_2} & \cdots & \frac{\partial f_2}{\partial x_n} \\ \vdots & \vdots & \ddots & \vdots \\ \frac{\partial f_n}{\partial x_1} & \frac{\partial f_n}{\partial x_2} & \cdots & \frac{\partial f_n}{\partial x_n} \end{bmatrix},$$

where f_i are the terms in the nonlinear vector \mathbf{f} and x_i are the states. Then $D_{\mathbf{x}^*}\mathbf{f}$ is found by substituting the state values at \mathbf{x}^* into the Jacobian expression. For autonomous systems, this matrix is usually just a constant matrix, in which case we define $D_{\mathbf{x}^*}\mathbf{f} = A$ where A is a $n \times n$ matrix of constant terms. Substituting this into Eq. (2.9) using Eq. (2.11) and ignoring the higher-order terms gives

$$\frac{d\xi}{dt} = A\xi, \quad (2.12)$$

which is a linear system, valid only as an approximation to the nonlinear system close to the equilibrium point, i.e. for ξ ‘small’.

2.2 Systems with Two States

Now consider the case when the system has two states, $\mathbf{x} = \{x_1, x_2\}^T$ and it is required to solve Eq. (2.12) close to an equilibrium point $\mathbf{x}^* = \{x_1^*, x_2^*\}^T$. To solve Eq. (2.12) we assume a solution of the form $\xi(t) = \mathbf{c}e^{\lambda t}$, where $\mathbf{c} = \{c_1, c_2\}^T$ is a vector of arbitrary constants.¹² Substituting this into Eq. (2.12) gives

$$\mathbf{c}\lambda e^{\lambda t} = A\mathbf{c}e^{\lambda t} \quad \text{so that} \quad \mathbf{c}\lambda = A\mathbf{c} \quad \text{or} \quad (A - \lambda I)\mathbf{c} = 0. \quad (2.13)$$

This is a linear eigenvalue problem, where λ are the eigenvalues. For Eq. (2.13) to be satisfied either $\mathbf{c} = 0$ or $\det(A - \lambda I) = 0$. The $\mathbf{c} = 0$ case involves no dynamics, so attention is focused on solving $\det(A - \lambda I) = 0$. For a two-dimensional system, this can be written as

¹¹ In fact, the formal definition is that the equilibrium points are *hyperbolic*. The structure of the trajectories close to a hyperbolic equilibrium point are topologically equivalent to the trajectory structure of the linearized dynamical system, see Guckenheimer and Holmes (1983) for a detailed discussion.

¹² An alternative approach is to use the solution $\xi = \xi_0 e^{At} = \xi_0 P e^{Jt} P^{-1}$ where J is the Jordan normal form of A —see for example Glendinning (1994).

$$\det \begin{bmatrix} a_{11} - \lambda & a_{12} \\ a_{21} & a_{22} - \lambda \end{bmatrix} = 0,$$

which when multiplied out becomes

$$\lambda^2 - (a_{11} + a_{22})\lambda + (a_{11}a_{22} - a_{21}a_{12}) = 0. \quad (2.14)$$

This is the characteristic equation and $(a_{11} + a_{22}) = \text{tr}(A)$ is called the *trace* of A and $(a_{11}a_{22} - a_{21}a_{12}) = \det(A)$ is the *determinant* of A . So now Eq. (2.14) can be rewritten as

$$\lambda^2 - \text{tr}(A)\lambda + \det(A) = 0,$$

which has the solution

$$\lambda_{1,2} = \frac{1}{2}(\text{tr}(A) \pm (\text{tr}(A)^2 - 4\det(A))^{\frac{1}{2}}). \quad (2.15)$$

Let $\text{tr}(A)^2 - 4\det(A) = \Delta$, where Δ is called the *discriminant*, then the eigenvalue solutions can be written as

$$\lambda_{1,2} = \frac{1}{2}(\text{tr}(A) \pm (\Delta)^{\frac{1}{2}}).$$

The sign of Δ determines whether the eigenvalues are real $\Delta > 0$, complex $\Delta < 0$ or repeated $\Delta = 0$. The signs of $\lambda_{1,2}$ are significant in determining the type of equilibrium points.

2.2.1 Equilibrium Points for Linear Harmonic Oscillator

Now consider the linear harmonic oscillator defined by $m\ddot{x} + c\dot{x} + kx = F(t)$, Eq. (1.3). First set the forcing parameter, $F(t)$, to zero so that the state space representation, Eq. (2.4), becomes

$$\begin{bmatrix} \dot{x}_1 \\ \dot{x}_2 \end{bmatrix} = \begin{bmatrix} 0 & 1 \\ -\frac{k}{m} & -\frac{c}{m} \end{bmatrix} \begin{bmatrix} x_1 \\ x_2 \end{bmatrix}. \quad (2.16)$$

Provided that all the parameters are non-zero, this system has a single equilibrium point at $x_1 = x_2 = 0$. Physically this is because, for an unforced, but damped, linear oscillator, releasing the mass from any non-zero displacement and velocity values results in the system gradually losing energy until it reaches the ‘at rest’ (zero displacement and velocity) point. The at rest position corresponds to the equilibrium point $x_1 = x_2 = 0$ in Eq. (2.16). The starting values are called the *initial conditions* and are values of displacement $x_1(0) = x(t = 0)$ and velocity $x_2(0) = \dot{x}(t = 0)$ at

time $t = 0$. For all initial $x_1(0), x_2(0) \neq 0$ values, the solution curves end up at the equilibrium point, and so the equilibrium point is said to be *attracting*.

From Eq. (2.16) the $\text{tr}(A) = -c/m$, $\det(A) = k/m$, $\Delta = (c^2 - 4km)/m^2$ and

$$\lambda_{1,2} = -\frac{c}{2m} \pm \frac{1}{2m} \sqrt{c^2 - 4km}.$$

Now consider the case when $\Delta < 0$. This means that the eigenvalues, $\lambda_{1,2}$ are complex, which physically corresponds to underdamped vibrations. Using the relationships $\omega_n = \sqrt{k/m}$ as the undamped natural frequency, $\zeta = c/2m\omega_n$ as the damping ratio and $\omega_d = \omega_n \sqrt{1 - \zeta^2}$ as the damped natural frequency, we can write the eigenvalues as $\lambda_{1,2} = -\zeta\omega_n \mp i\omega_d$. Substituting this into the original assumed solution, $\xi(t) = \mathbf{c}e^{\lambda t}$ results in a solution which can be expressed as

$$\xi(t) = \mathbf{c}e^{-\zeta\omega_n t} \sin(\omega_d t).$$

This is a sine wave oscillation multiplied by an exponential envelope. There are two cases, depending on whether the damping is positive ($c > 0$ therefore $\zeta > 0$) or negative ($c < 0$ therefore $\zeta < 0$). The two cases are shown in Fig. 2.5a, c in terms of time history plots. For $\zeta > 0$ (Fig. 2.5a), the exponential envelope causes the sinusoidal oscillation to decay, but when $\zeta < 0$ (Fig. 2.5c) the oscillations grow. These two types of behaviour can be plotted in the state space x_1 versus x_2 , which is shown in Fig. 2.5b, d relative to the equilibrium point at the origin.

Figure 2.5b is known as a *stable spiral* (or a focus or sink), and Fig. 2.5d is an *unstable spiral* (or a repeller or source). The idea of stability can be related to whether the oscillations grow or decay. If they decay, such that solution curves of the governing equation of motion are *attracted* to the equilibrium point, then this is

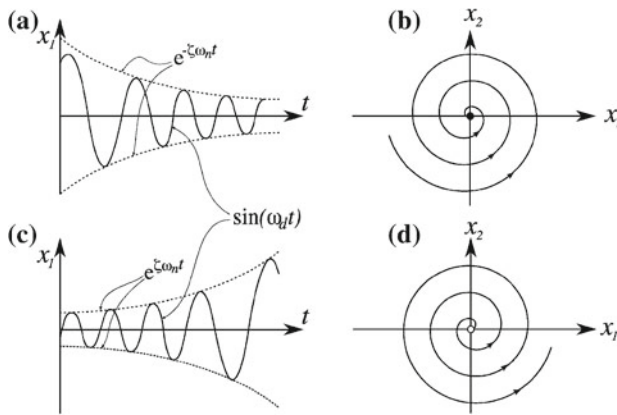


Fig. 2.5 Local equilibrium point dynamics showing **a** positive damping corresponding to **b** a stable spiral, and **c** negative damping, which corresponds to **d** an unstable spiral

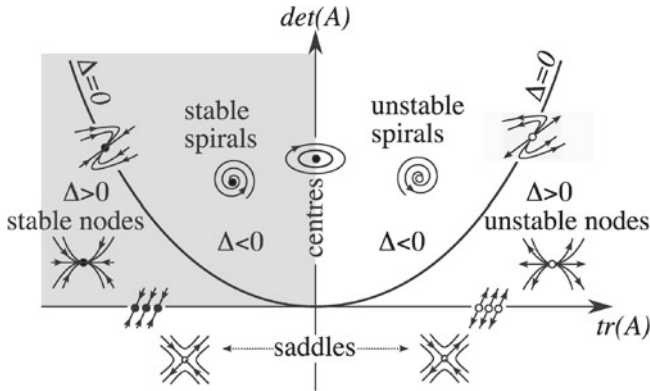


Fig. 2.6 Type and local stability of equilibrium points for a two state linear(ised) system

a stable behaviour. If the oscillations grow such that solution curves of the governing equation of motion are *repelled* from the equilibrium point, then this is an unstable behaviour.

Figure 2.6 shows the relationship between $\text{tr}(A)$, $\det(A)$, Δ and the type and stability of all equilibrium points for the linear oscillator with two states, $x = \{x_1, x_2\}^T$. From a physical perspective (at least for this book) the mass, m , is always a positive constant. But both the stiffness and damping can be either positive or negative constants. In Fig. 2.6 the upper left-hand quadrant is shaded grey to indicate the region of *stable* solutions. The physical nature of the *unstable* regions corresponds to solutions with negative damping and negative stiffness. For constant, positive mass, the $\text{tr}(A)$ is proportional to the damping, c , and $\det(A)$ is proportional to the stiffness, k . So $\det(A) < 0$ corresponds to negative stiffness $k < 0$, and from Fig. 2.6 it can be seen that this corresponds to saddle solutions. In addition $\text{tr}(A) > 0$ corresponds to negative damping $c < 0$. The transition from the stable quadrant as damping changes sign can be thought of as a *dynamic instability*. Conversely, the transition that occurs as stiffness becomes negative is a form of *static instability*.

Notice that in the stable quadrant all solution curves have arrows pointing towards the equilibrium point. The equilibrium points are also shown as solid black dots, indicating that these equilibrium points are stable and *attract* solution curves toward them. The unstable quadrants have at least some of the solution curves pointing away from the equilibrium point, and the open circles indicate that the equilibrium points are unstable, and *repel* solution curves. The concept of stability will be discussed in further detail in Sect. 2.5.

The nodes shown in Fig. 2.6 correspond to the case when the eigenvalues are real and distinct. Physically this corresponds to the case when $\Delta = (c^2 - 4km)/m^2 > 0$ which is otherwise known as the overdamped case, i.e. when $\zeta > 1$, and will not be discussed in detail here—see Inman (2006) for a discussion on linear overdamped vibration.

Figure 2.6 also shows three special types of behaviour (i) when $\text{tr}(A) = 0$, (ii) when $\det(A) = 0$, and (iii) when $\Delta = 0$. The last case, when $\Delta = 0$ corresponds to

a critically damped system, $\zeta = 1$, so that $\lambda_1 = \lambda_2$ and the behaviour is known as a degenerate (or inflected) node.¹³ When $\det(A) = 0$ the transition to static instability occurs as the stiffness passes through zero. In this case the origin is not an isolated equilibrium point, instead a whole line of equilibrium points exists, see Strogatz (2001). The case when $\text{tr}(A) = 0$ corresponds to zero damping, and the positive half of the $\det(A)$ axis in Fig. 2.6 (where $\text{tr}(A) = 0$) represents the transition from stable to unstable spirals. This is by far the most important degenerate case for vibration analysis, as it corresponds to the zero damping case. For vibration systems with small damping, the zero damping case is often used to provide a simplified analysis of the system behaviour.¹⁴ An example of finding equilibrium point behaviour is considered next.

Example 2.3 Equilibrium points for an oscillator with quadratic stiffness nonlinearity (the escape equation)

Problem Find the type and stability of the equilibrium points for the following equation with a quadratic nonlinear term

$$m\ddot{x} + c\dot{x} + k_1x + k_2x^2 = 0,$$

with mass $m = 1$ kg, damping $c = 0.1$ Ns/m, linear stiffness $k_1 = 1$ N/m and quadratic stiffness $k_2 = 1$ N/m². This equation is sometimes referred to as the *escape equation*.

Solution First, put the system into first-order form by defining $x_1 = x$ and $x_2 = \dot{x}$, such that $\ddot{x} = \dot{x}_2$. This gives

$$\begin{aligned}\dot{x}_1 &= x_2 = f_1, \\ \dot{x}_2 &= -(0.1)x_2 - x_1 - x_1^2 = f_2.\end{aligned}\tag{2.17}$$

The equilibrium points are values of (x_1, x_2) which make the right-hand side of Eq. (2.17) equal to zero ($\mathbf{f} = 0$, which means that $f_1 = 0$, $f_2 = 0$). So, by inspection it can be seen that $(x_1 = 0, x_2 = 0) = \mathbf{x}_a^*$ is an equilibrium point. Note that x_2 must always be zero to satisfy the first line of Eq. (2.17), $f_1 = 0$. When $x_2 = 0$, the second line of Eq. (2.17) gives $f_2 = -x_1 - x_1^2 = 0$ from which $x_1 = -1$ is a solution, so there is a second equilibrium point at $(x_1 = -1, x_2 = 0) = \mathbf{x}_b^*$.

¹³ In fact the behaviour depends on the *multiplicity* of the repeated eigenvalue. The degenerate node corresponds to the case where there is only a single eigenvector. For the case with two eigenvectors the degenerate equilibrium point becomes a *star* see Strogatz (2001). See Seyranian and Mailybaev (2003) for a more detailed discussion of multiplicity.

¹⁴ When $\text{tr}(A) = 0$ and $\det(A) = 0$, there is a doubly-degenerate equilibrium point. This is not discussed further here.

To find the type and stability of the equilibrium points, the Jacobian, $D_{\mathbf{x}^*}\mathbf{f}$, must be determined for each equilibrium point. The Jacobian of Eq. (2.17) is

$$D_{\mathbf{x}}\mathbf{f} = \frac{\partial(f_1, f_2)}{\partial(x_1, x_2)} = \begin{bmatrix} \frac{\partial f_1}{\partial x_1} & \frac{\partial f_1}{\partial x_2} \\ \frac{\partial f_2}{\partial x_1} & \frac{\partial f_2}{\partial x_2} \end{bmatrix} = \begin{bmatrix} 0 & 1 \\ -1 - 2x_1 & -0.1 \end{bmatrix}. \quad (2.18)$$

Now substitute each of the equilibrium points into the Jacobian in turn. First for $\mathbf{x}_a^* = (x_1 = 0, x_2 = 0)$ the transformed localized coordinates are $\xi_1 = x_1 - 0 = x_1$ and $\xi_2 = x_2 - 0 = x_2$. The Jacobian becomes

$$D_{\mathbf{x}_a^*}\mathbf{f} = \begin{bmatrix} 0 & 1 \\ -1 & -0.1 \end{bmatrix}. \quad (2.19)$$

As $D_{\mathbf{x}_a^*}\mathbf{f}$ is a constant matrix, define $D_{\mathbf{x}_a^*}\mathbf{f} = A$. From Eq. (2.19), the trace of $D_{\mathbf{x}_a^*}\mathbf{f}$ is given by $\text{tr}(D_{\mathbf{x}_a^*}\mathbf{f}) = -0.1$ and the determinant is $\det(D_{\mathbf{x}_a^*}\mathbf{f}) = 1$. Recall from Eq. (2.15) that the discriminant, Δ is given by $\Delta = \text{tr}^2 - 4\det$. So for equilibrium point \mathbf{x}_a^* , the discriminant, $\Delta = -3.99$. Then using Fig. 2.6, it can be seen that this equilibrium point has negative $\text{tr}(A)$, positive $\det(A)$ and $\Delta < 0$. This means that the equilibrium point is a stable spiral.

For the equilibrium point \mathbf{x}_b^* , the localized coordinates are $\xi_1 = x_1 - (-1) = x_1 + 1$ and $\xi_2 = x_2 - 0 = x_2$. Substituting $\mathbf{x}_b^* = (x_1 = -1, x_2 = 0)$ into Eq. (2.18), the Jacobian becomes

$$D_{\mathbf{x}_b^*}\mathbf{f} = \begin{bmatrix} 0 & 1 \\ 1 & -0.1 \end{bmatrix}.$$

So in this case $\text{tr}(A) = -0.1$ and $\det(A) = -1$, which from Fig. 2.6 means that this equilibrium point is a saddle. ■

2.3 The Link Between State Space and Mechanical Energy

Consider an unforced linear oscillator with negligible damping such that the system is approximated as being undamped, in which case

$$m\ddot{x} + kx = 0,$$

where k is the spring stiffness and x is the displacement of the mass, m . Considering the work done over a small increment of distance dx , as the mass moves from resting $x = 0$ to an arbitrary x value gives the integral

$$\int_0^x (m\ddot{x} + kx)dx = m \int_0^x \ddot{x}dx + k \int_0^x xdx = E_t, \quad (2.20)$$

where E_t is the total energy. Note that velocity, $v = \frac{dx}{dt}$ and acceleration $\frac{d^2x}{dt^2} = \frac{dv}{dt}$ so that $\frac{dv}{dt}dx = vdv$, which can be substituted into Eq. (2.20) (with a change of integration limits) to give

$$m \int_0^v vdv + k \int_0^x xdx = \frac{1}{2}mv^2 + \frac{1}{2}kx^2 = E_t. \quad (2.21)$$

Equation (2.21) represents the kinetic plus potential energy of the mass-spring system, where $\frac{1}{2}mv^2$ is the kinetic and $\frac{1}{2}kx^2$ is the potential energy.

Equation (2.21) also represents the *Hamiltonian* for the system. For dynamical systems, Hamiltonians are typically used to model systems that are undamped,¹⁵ also called *conservative* as energy is conserved. In vibration analysis of mechanical systems, applications are typically *non-conservative*, as damping is nearly always present. However, when damping is small, analysis is often developed for the undamped system, as the results are very close to (but not exactly the same) as for the system with damping.¹⁶

2.3.1 Potential Functions

Now a direct link can be made between the system state space and the energy in the system. To see this, first notice that in terms of state variables the velocity, $v = \dot{x} = x_2$ and the displacement $x = x_1$. Now consider the unforced, undamped nonlinear oscillator

$$m\ddot{x} + p(x) = 0 \rightsquigarrow mv \frac{dv}{dx} + p(x) = 0,$$

where $p(x)$ is the stiffness function. Integrating to find the energy gives

$$\frac{1}{2}mv^2 + \int_0^x p(x) = E_t \rightsquigarrow \frac{1}{2}mv^2 + V(x) = E_t, \quad (2.22)$$

where $V(x) = \int_0^x p(x)$ is called the *potential* function.¹⁷

¹⁵ See, for example, Guckenheimer and Holmes (1983) and Strogatz (2001) for an introduction and further references.

¹⁶ The fact that the undamped solutions *persist* with the addition of small damping, is an important underlying assumption in vibration analysis.

¹⁷ Not to be confused with potential energy.

As an example, consider the generic version of the escape equation, from Example 2.3. The equation of motion is given by

$$m\ddot{x} + c\dot{x} + k_1x + k_2x^2 = 0,$$

where m is mass, c the damping, k_1 is linear stiffness and k_2 nonlinear stiffness. In this case $p(x) = k_1x + k_2x^2$, such that the potential function $V(x)$ is given by

$$V(x) = \int_0^x (k_1x + k_2x^2)dx = \frac{1}{2}k_1x^2 + \frac{1}{3}k_2x^3. \quad (2.23)$$

Example 2.4 Phase portrait for the undamped escape equation

Problem Construct the phase portrait and potential function for the unforced, undamped escape equation given by

$$m\ddot{x} + kx + k_2x^2 = 0, \quad (2.24)$$

where $m = 1$ kg, $k = 1$ N/m and $k_2 = 1$ N/m².

Solution First put the system into first-order form by defining $x_1 = x$ and $x_2 = \dot{x}$, such that $\ddot{x} = \dot{x}_2$. This gives

$$\begin{aligned} \dot{x}_1 &= x_2 = f_1, \\ \dot{x}_2 &= -x_1 - x_1^2 = f_2. \end{aligned}$$

The equilibrium points for this system are $\mathbf{x}_a^* = (x_1 = 0, x_2 = 0)$ and $\mathbf{x}_b^* = (x_1 = -1, x_2 = 0)$. The Jacobian is

$$D_{\mathbf{x}}\mathbf{f} = \frac{\partial(f_1, f_2)}{\partial(x_1, x_2)} = \begin{bmatrix} \frac{\partial f_1}{\partial x_1} & \frac{\partial f_1}{\partial x_2} \\ \frac{\partial f_2}{\partial x_1} & \frac{\partial f_2}{\partial x_2} \end{bmatrix} = \begin{bmatrix} 0 & 1 \\ -1 - 2x_1 & 0 \end{bmatrix}.$$

First, for $\mathbf{x}_a^* = (x_1 = 0, x_2 = 0)$, the Jacobian becomes

$$D_{\mathbf{x}_a^*}\mathbf{f} = \begin{bmatrix} 0 & 1 \\ -1 & 0 \end{bmatrix},$$

and localized coordinates $\xi_1 = x_1$ and $\xi_2 = x_2$. So for equilibrium point \mathbf{x}_a^* , $\text{tr}(A) = 0$ and $\det(A) = 1$ which using Fig. 2.6 is a centre. For equilibrium point $\mathbf{x}_b^* = (x_1 = -1, x_2 = 0)$, the Jacobian becomes

$$D_{\mathbf{x}_b^*}\mathbf{f} = \begin{bmatrix} 0 & 1 \\ 1 & 0 \end{bmatrix},$$

and localized coordinates $\xi_1 = x_1$ and $\xi_2 = x_2$. So in this case $\text{tr}(A) = 0$ and $\det(A) = -1$ which from Fig. 2.6 means that this equilibrium point is a saddle point.

The potential function can be found from Eq. (2.23). In this example $k_1 = k_2 = 1$ and $x = x_1$, so

$$V(x) = \frac{1}{2}x^2 + \frac{1}{3}x^3. \quad (2.25)$$

The phase space and potential function are shown in Fig. 2.7. ■

Figure 2.7 shows the link between the phase portrait (x_1, x_2) and the potential function $V(x)$. Notice that in terms of the state variables, the energy of any solution curve, from Eqs. (2.22) and (2.25), is defined by

$$E_t = \frac{1}{2}mx_2^2 + k\frac{1}{2}x_1^2 + k_2\frac{1}{3}x_2^3.$$

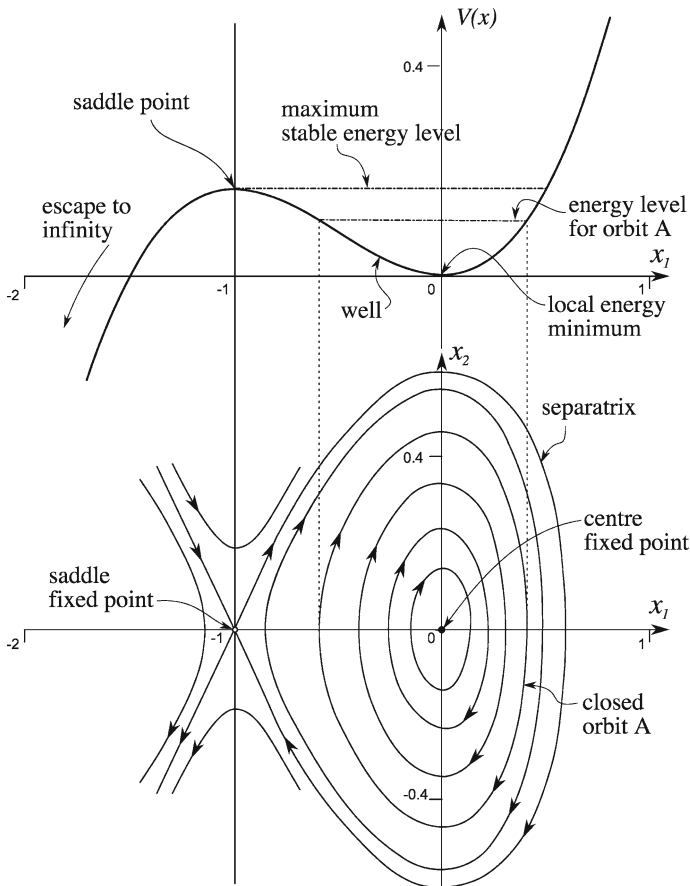


Fig. 2.7 Phase space and potential function for the undamped escape equation

So, on the x_2 axis, when $x_1 = 0$, the energy is purely kinetic $E_t = \frac{1}{2}mx_2^2$. This also corresponds to maximum and minimum x_2 values of any of the stable solution curves in the phase portrait, see for example, closed orbit A in Fig. 2.7. Conversely, when $x_2 = 0$, $E_t = V(x) = k_1\frac{1}{2}x_1^2 + k_2\frac{1}{3}x_1^3$, and maximum and minimum x_1 values for closed orbit A occur on the $x_2 = 0$ axis. The potential function, $V(x)$, is drawn in the top half of Fig. 2.7. This corresponds to the total energy along the x_1 axis. An example is shown for closed orbit A in the phase portrait (the lower part of Fig. 2.7), which has dashed lines from the intersections with the x_1 axis up to the energy plot. The constant energy level for closed orbit A is shown on the energy diagram.

As the size of the closed orbit increases, so does the energy level. At the point where the closed orbit touches the saddle point,¹⁸ it also reaches a maximum energy level. Beyond this point the system becomes unstable, and solutions *escape* to infinity, which means they become infinitely large. The closed orbit which goes through the saddle point is the separatrix,¹⁹ which in this case separates the stable area of solutions from the unstable area.

The stable part of the energy function containing the closed orbits is often called a *potential well*. Solutions which leave the potential well are sometimes said to have escaped from the potential well. From an engineering perspective, the escape phenomena are often related to catastrophic failure, for example, ship capsize or structural failure, Thompson and Stewart (2002).

Now consider an example of a system with a cubic nonlinear stiffness term.

Example 2.5 Phase portrait for oscillator with cubic stiffness nonlinearity (undamped Duffing oscillator)

Problem Construct the phase portrait and potential function for the unforced, undamped Duffing oscillator equation given by

$$m\ddot{x} - k_1x + k_3x^3 = 0, \quad (2.26)$$

with mass $m = 1$ kg, negative linear stiffness $k_1 = -1$ N/m and cubic stiffness $k_3 = 1$ N/m³.

Solution First put the system into first-order form by defining $x_1 = x$ and $x_2 = \dot{x}$, such that $\dot{x} = \dot{x}_2$. This gives

$$\begin{aligned} \dot{x}_1 &= x_2 = f_1, \\ \dot{x}_2 &= x_1 - x_1^3 = f_2. \end{aligned}$$

By inspection, the equilibrium points for this system are $\mathbf{x}_a^* = (x_1 = 0, x_2 = 0)$, $\mathbf{x}_b^* = (x_1 = 1, x_2 = 0)$ and $\mathbf{x}_c^* = (x_1 = -1, x_2 = 0)$. The Jacobian is

¹⁸ Also known as a homoclinic bifurcation.

¹⁹ Also known as a homoclinic orbit, an orbit which starts and finishes at the same saddle point. Not to be confused with a heteroclinic orbit, which joins two separate saddle points.

$$D_{\mathbf{x}}\mathbf{f} = \frac{\partial(f_1, f_2)}{\partial(x_1, x_2)} = \begin{bmatrix} \frac{\partial f_1}{\partial x_1} & \frac{\partial f_1}{\partial x_2} \\ \frac{\partial f_2}{\partial x_1} & \frac{\partial f_2}{\partial x_2} \end{bmatrix} = \begin{bmatrix} 0 & 1 \\ 1 - 3x_1^2 & 0 \end{bmatrix}.$$

For $\mathbf{x}_a^* = (x_1 = 0, x_2 = 0)$, the Jacobian becomes

$$D_{\mathbf{x}_a^*}\mathbf{f} = \begin{bmatrix} 0 & 1 \\ 1 & 0 \end{bmatrix}.$$

So for equilibrium point \mathbf{x}_a^* , $\text{tr}(A) = 0$ and $\det(A) = -1$ which using Fig. 2.6 is a saddle.

For equilibrium point $\mathbf{x}_b^* = (x_1 = 1, x_2 = 0)$, the Jacobian becomes

$$D_{\mathbf{x}_b^*}\mathbf{f} = \begin{bmatrix} 0 & 1 \\ -2 & 0 \end{bmatrix}, \quad (2.27)$$

so in this case $\text{tr}(A) = 0$ and $\det(A) = 2$, which from Fig. 2.6 means that this equilibrium point is a centre. Equilibrium point $\mathbf{x}_c^* = (x_1 = -1, x_2 = 0)$ has the same Jacobian as equilibrium point \mathbf{x}_b^* , Eq. (2.27), and is also a centre.

The potential function can be found by integrating Eq. (2.26). In this example $p(x_1) = -x_1 + x_1^3$, so

$$V(x_1) = -\frac{1}{2}x_1^2 + \frac{1}{3}x_1^3 + \frac{1}{4},$$

where the $\frac{1}{4}$ constant ensures that the potential function is always positive, i.e. $V(x_1) \geq 0$ for all x_1 . The phase space and potential functions are shown in Fig. 2.8. ■

Notice that the system plotted in Fig. 2.8 actually has a negative linear stiffness, $k_1 = -1$, which explains why there is a saddle point at the origin. This type of system may at first seem to have limited physical applications, but it can be used to model an interesting class of systems which have bi-stability. Or, in other words, they have two stable configurations (like the two equilibrium points at ± 1 in Fig. 2.8) separated by an unstable configuration (the saddle in Fig. 2.8). Classic examples are, buckled beams (discussed in Sect. 2.6), curved plates which can *snap-through* from one stable configuration to another (discussed in Chap. 8), and a cantilever beam with two magnetic fields acting on the tip—the so-called *Moon beam* (Moon 1987).

The form of $V(x)$ shown in Fig. 2.8 is often called a double potential well. The sides of the well continue to extend upwards, and energy levels for two different orbits are shown in Fig. 2.8. Orbit A is inside the potential well around the equilibrium point at $x_1 = 1, x_2 = 0$. Orbit B has a much higher energy level and is not confined to either of the centre equilibrium points. Here the separatrix marks the boundary between (i) the orbits confined to the potential wells around each of the centre equilibrium points and (ii) orbits which enclose both.

An analogy that is often used is to imagine that at any point in time the state of the system is represented by a ball rolling on the energy surface. As time evolves, the

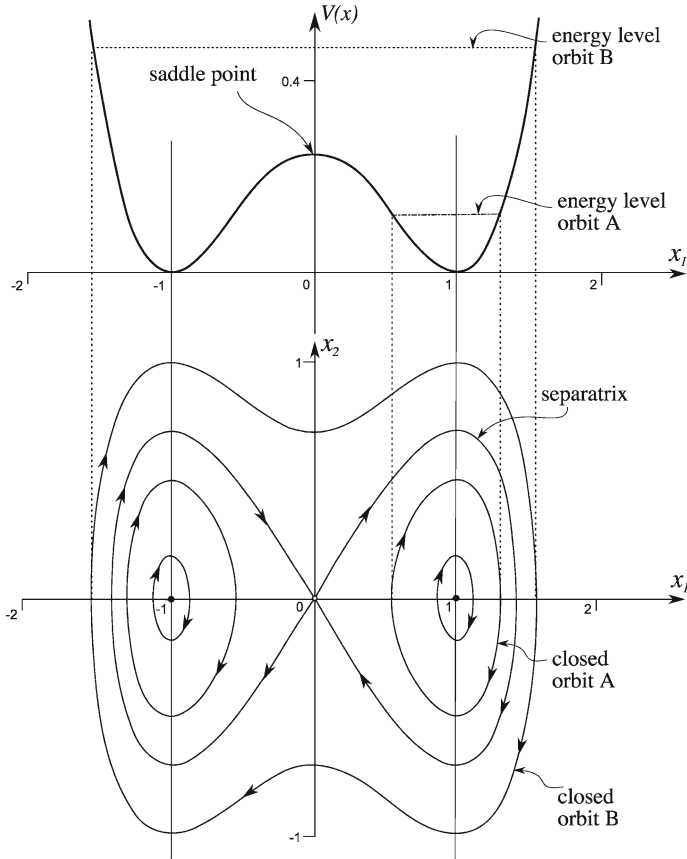


Fig. 2.8 Phase space and potential function for the undamped Duffing oscillator

ball will trace out a particular orbit in phase space, which in the case of an undamped, unforced system, would mean that the ball is constrained to be at a constant level on the energy surface—neither gaining or losing energy.

If the energy level can vary, then points where the ball crosses the separatrix correspond to the system escaping from one well into another, or—for the escape equation—to infinity. A further analogy is to imagine the phase space orbits as contours. These contours indicate lines of constant energy, in a similar way that contours on a map indicate lines of constant height. By interpreting the phase portrait in this way an image of the energy surface, and therefore the system dynamics, can be obtained. This is shown in Fig. 2.9, which shows the complete energy surface for the Duffing oscillator example, Example 2.5. Extending the energy function in the x_2 direction gives a parabolic shape which can be seen from Eq. (2.22) where

$$E_t = V(x) + \frac{1}{2}mx_2^2.$$

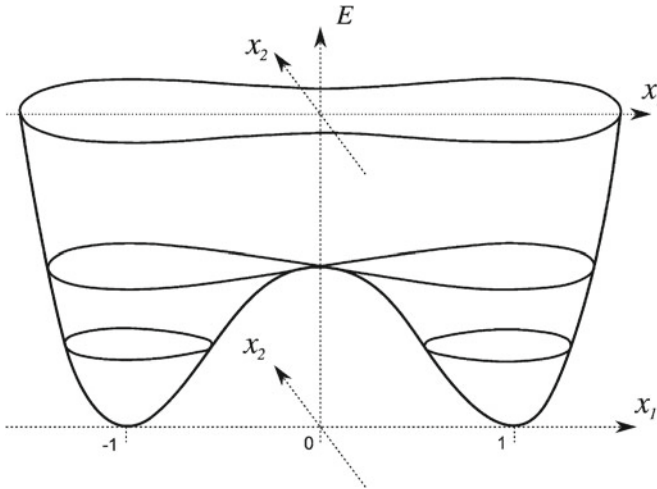


Fig. 2.9 Total energy surface for the Duffing oscillator

2.4 Multiple Solutions, Stability and Initial Conditions

A clear difference between linear oscillations and nonlinear oscillations is that nonlinear systems can have multiple solutions. For example, for the negative linear stiffness Duffing oscillator considered in Example 2.5, there are two stable equilibrium points, one at $x_1 = -1$ and the other at $x_1 = 1$. When damping is added to the system, these equilibrium points become attracting spirals, and the phase portrait changes to that shown in Fig. 2.10. This means that for a particular choice of initial conditions, $x_1(t_0)$, $x_2(t_0)$, there are two potential finishing points. In fact, the regions of initial starting points for each stable equilibrium point are defined by the outer trajectories in Fig. 2.10. Starting points which are close to each other, but on either side of the saddle's *stable manifold*,²⁰ will diverge at the saddle point (due to the effect of the *unstable manifolds* coming out of the saddle point) and finish at different equilibrium points. An example is shown in Fig. 2.11, where two trajectories with initially close starting points²¹ are attracted to different equilibrium points.

To find the initial condition values that are attracted to an equilibrium point for a whole region of initial values, the technique of *cell-to-cell mapping* can be used. This is a numerical technique which divides up the region of potential initial conditions into a grid. Each point in the grid is then used as an initial condition point, and a mapping from one cell to the next computed until an equilibrium point is reached. Each starting point is plotted (usually as a colour) based on which equilibrium point it is attracted to. Using this technique the *basins of attraction* can be seen. These are the regions of initial conditions which lead to trajectories which finish at the equilibrium

²⁰ This is the separatrix trajectory which goes directly to the saddle point.

²¹ In fact they could be closer, but they have been slightly separated to make the figure clearer.

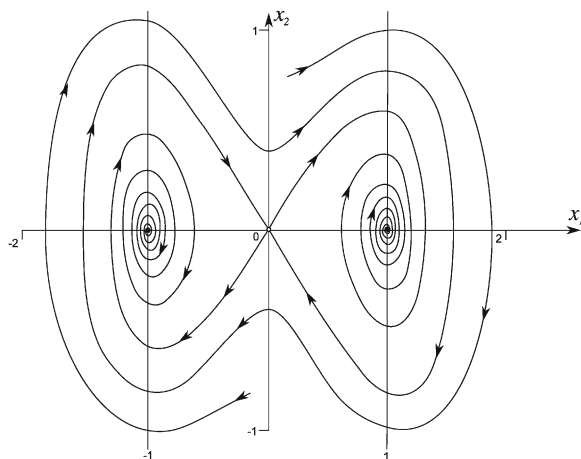


Fig. 2.10 Duffing oscillator phase portrait with damping

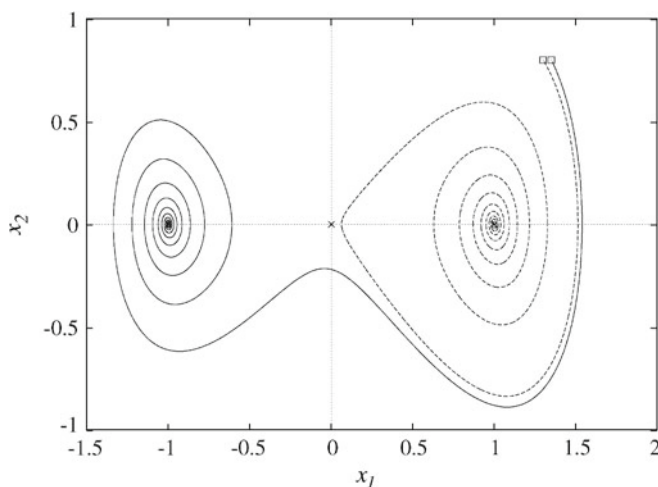


Fig. 2.11 Two close starting points finishing at different equilibrium points

point. These basins of attraction define the eventual, steady-state, behaviour of the oscillator. Using the same approach, but recording the *time taken* to reach a steady-state, can give information about the transient behaviour of the oscillator.

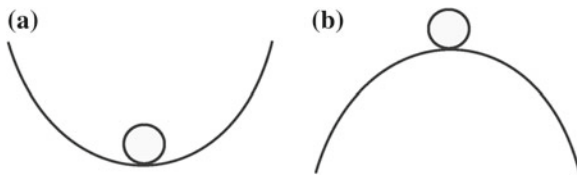


Fig. 2.12 Basic concept of stability. **a** Stable. **b** Unstable

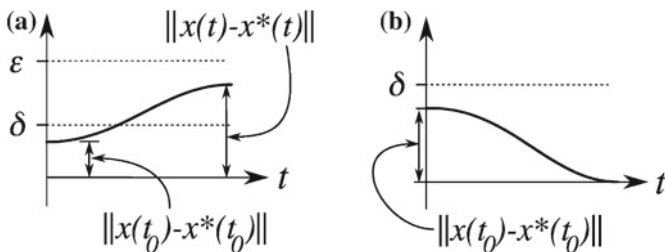


Fig. 2.13 Stability for a single state dynamical system, showing **a** Lyapunov stable, **b** asymptotically stable

2.4.1 Stability

In Sect. 2.1.3 attracting equilibrium points were said to be stable, but how is stability defined? The basic concept of stability can be visualized by considering a ball rolling over a surface. This is shown in Fig. 2.12 where an unstable position corresponds to the ball on a hill top, and a stable position corresponds to a ball resting in the bottom of a well. Any small disturbance will cause the ball on the hill top to roll down, whereas a small disturbance to the ball in the well would, under gravity, cause it to roll back to its original position.

In more precise terms it can be said that an equilibrium point, \mathbf{x}^* , is stable if a solution, $\mathbf{x}(t)$, close to it remains close for all time t . For example, for the system

$$\frac{d\mathbf{x}}{dt} = \mathbf{f}(\mathbf{x}, t), \quad \mathbf{x}(t_0) = \mathbf{x}_0,$$

an equilibrium point, \mathbf{x}^* , is *Lyapunov stable* if $\|\mathbf{x}(t_0) - \mathbf{x}^*(t_0)\| < \delta \Rightarrow \|\mathbf{x}(t) - \mathbf{x}^*(t)\| < \epsilon$, which is shown in Fig. 2.13a for a single state system. In other words, an equilibrium point is Lyapunov stable if trajectories that are initially close remain close. The idea of closeness is defined by δ and ϵ . For a choice of δ , the trajectory never goes further than ϵ if the system is to be Lyapunov stable. This type of stability is also called neutral stability. It includes centre equilibrium points where orbits stay close, but are neither pulled toward or pushed away from the equilibrium point.

An equilibrium point is *asymptotically* stable if nearby trajectories are ‘attracted’ to it as $t \rightarrow \infty$. This is written as $\|\mathbf{x}(t_0) - \mathbf{x}^*(t_0)\| < \delta \Rightarrow \lim_{t \rightarrow \infty} \|\mathbf{x}(t) - \mathbf{x}^*(t)\| = 0$, which is shown in Fig. 2.13b. This type of stability applies to stable nodes and stable spirals, where nearby orbits are pulled strongly towards the equilibrium point.

2.5 Periodic and Non-periodic Oscillations

For unforced, undamped systems, steady-state periodic orbits can be observed which have amplitudes that are dependent on the initial conditions. However, the vast majority of mechanical engineering systems of interest are both forced and damped. For these systems, a common steady-state response is a periodic orbit with the same period as the harmonic forcing function. The response amplitudes will depend on the energy balance in the system. These types of periodic orbits are called *limit cycles* as noted in Example 2.1. Unlike the unforced, undamped case, where there are an infinite number of steady-state orbits which depend on the initial conditions, limit cycles are not entirely dependent on initial values. In fact they have the property of attracting nearby solution trajectories in state space. An example is shown in Fig. 2.14.

In addition to limit cycles it is possible to encounter a range of other types of behaviour. For example a closed orbit that takes two forcing periods to repeat the motion is called a *period-two* orbit. In fact multiple periodic responses can often be found and in general they are denoted as period n orbits.

Non-periodic responses can also occur, including *quasi-periodic* motion and *chaos*. Quasi-periodic motion (meaning almost, but not quite periodic) occurs when the response is composed of two or more signals with frequencies which are not-integer multiples of each other. In fact this type of motion can occur regularly in

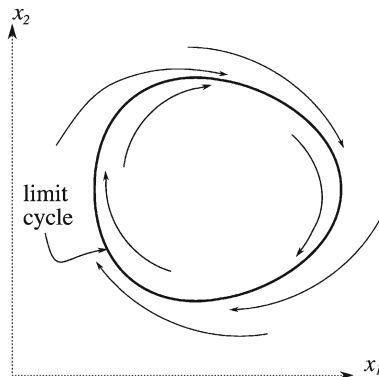


Fig. 2.14 A stable limit cycle oscillation which attracts nearby transient trajectories

vibration problems with multiple frequencies in the response. Linear natural frequencies are typically non-integer multiples, but they are spaced such that vibration modes at other frequencies are less significant to the response. However, closely spaced modes can result in a multi-frequency response which can appear similar to a quasi-periodic response for a nonlinear single degree-of-freedom system.

Viewed as a time series, chaos often appears to be non-repeatable and non-deterministic, but is in fact highly structured. However, how can chaos be identified as different from quasi-periodic or random time signals? Chaos is characterized by being highly sensitive to initial conditions, so that a very small change, leads to a very quick divergence of behaviour. This divergence can be quantified by calculating the rate of separation of initially close starting points as time increases. The rate of exponential divergence between nearby trajectories is measured by the *Lyapunov exponents* for the system. So if $\delta(t_0)$ is the initial distance between two nearby trajectories at the starting time t_0 , and at some later time, t , the distance is modelled by $\delta(t) = e^{\lambda t} \delta(t_0)$, then λ is the Lyapunov exponent. For the general case where there would typically be more than one Lyapunov exponent, and one or more of the exponents is positive, then trajectories are separating with positive *exponential divergence*, and the system is chaotic. Exponential divergence is a key indication that the system is deterministic chaos, rather than a time signal from a stochastic system. This is because in a stochastic system trajectory separation is typically random rather than exponentially diverging.

A further test is to look at the data in the frequency domain. Chaos typically has a broad frequency content, as opposed to clear resonant peaks or harmonics from other non-chaotic signals. An example of this is discussed below.

In vibration analysis, chaos generally appears readily in low-dimensional problems, typically in forced nonlinear oscillators, such as the Duffing oscillator. In more flexible structures, which naturally have multiple modes, chaos is less readily apparent, and more difficult to distinguish as a specific response—especially when damping is very light. It should also be noted that chaos has primarily been studied and classified for low-dimensional problems with a single harmonic forcing input, which limits its relevance to higher-dimensional vibration problems. In some applications, chaos is seen as a desirable response—for example to distribute wear evenly across mechanical components—but in most vibration applications it is seen as undesirable, mainly because it typically has much larger amplitudes and is much less predictable than periodic motions. An example showing periodic and non-periodic responses is considered next.

Example 2.6 Periodic and non-periodic oscillations in a damped Duffing oscillator

Problem Consider the following forced, damped Duffing oscillator with negative linear stiffness

$$\ddot{x} + 0.4\dot{x} - x + x^3 = F \cos(1.8t), \quad (2.28)$$

where F is the forcing amplitude. Use time series and frequency spectra to investigate what type of periodic and non-periodic behaviour this oscillator has for F in the range $0.6 \leq F \leq 1.8$.

Solution Equation (2.28) can be written in first-order form

$$\begin{aligned}\dot{x}_1 &= x_2, \\ \dot{x}_2 &= -(0.4)x_2 + x_1 - x_1^3 + F \cos(1.8t).\end{aligned}$$

The dynamics of this first-order system can now be simulated by first computing time series from initial values (this is typically done using 4th-order Runge-Kutta numerical integration as mentioned in Example 2.1). The simplest way to examine the behaviour for a range of F values is just to select some across the given range. Four cases of the dynamics of the forced Duffing oscillator with forcing values in the range $0.6 \leq F \leq 1.8$ have been computed and are shown in Fig. 2.15. The four cases selected are; $F = 0.6$ shown in (a1)–(a3), $F = 0.73$ shown in (b1)–(b3), $F = 1.51$ shown in (c1)–(c3) and $F = 1.8$ shown in (d1)–(d3). In each case the left-hand picture shows the time series at the selected F value. Then in the centre the corresponding steady-state attractor in the (x, \dot{x}) plane is shown for each case. Finally on the right-hand side, the frequency spectrum is shown.

The frequency spectrum is obtained by taking the Fourier transform (FFT) of the time series and then using the absolute value of FFT amplitude, X . The log (to base 10) of $|X|$ is plotted against a linear scale of frequencies in Hz. Logs of the amplitudes are used so that all relevant frequency content can be viewed in the plot.²² The angular forcing frequency in this example is $\omega = 1.8$ rad/s, which is related to the frequency, f , in Hz, by the relation $\omega = 2\pi f$, so that $f = 0.286$ in this case. The position of f in the frequency spectrum is marked on Fig. 2.15a3–d3 with an arrow. Frequency peaks at integer multiples of f from 1 to 5 are also marked on the frequency spectrum.

In the first case, $F = 0.6$ shown in (a1)–(a3), the motion repeats after one forcing period. The response is periodic but non-harmonic. As a result, in the frequency spectrum, as well as a response at f , the second and third harmonics are clearly evident. Notice also that the time series is not centred at zero displacement. This leads to a significant value in the frequency spectrum at zero, which is sometimes called the DC offset.²³

In the second case, $F = 0.73$ shown in (b1)–(b3), the motion repeats after three forcing periods. As before this is periodic but non-harmonic and, in the frequency spectrum, multiple response peaks are evident. However, in this case only 1 and 3 are integer harmonics of f . The peak lower in the spectrum than f is a $1/3$ *subharmonic*. Other peaks correspond to non-integer harmonics at $5/3$, $7/3$, $11/3$ and $13/3$.

In the third case, $F = 1.51$ shown in (c1)–(c3), the motion repeats after four forcing periods. Now, in the frequency spectrum all the integer harmonics from 1 to

²² There is a range of alternatives for plotting frequency spectra, the most common of which are various definitions of *power spectra*. Further discussion of the merits of these methods can be found in Newland (1993) and Press et al. (1994).

²³ This term originates from electronics, where it refers to a direct current voltage, but the concept has been extended to any representation of a waveform.

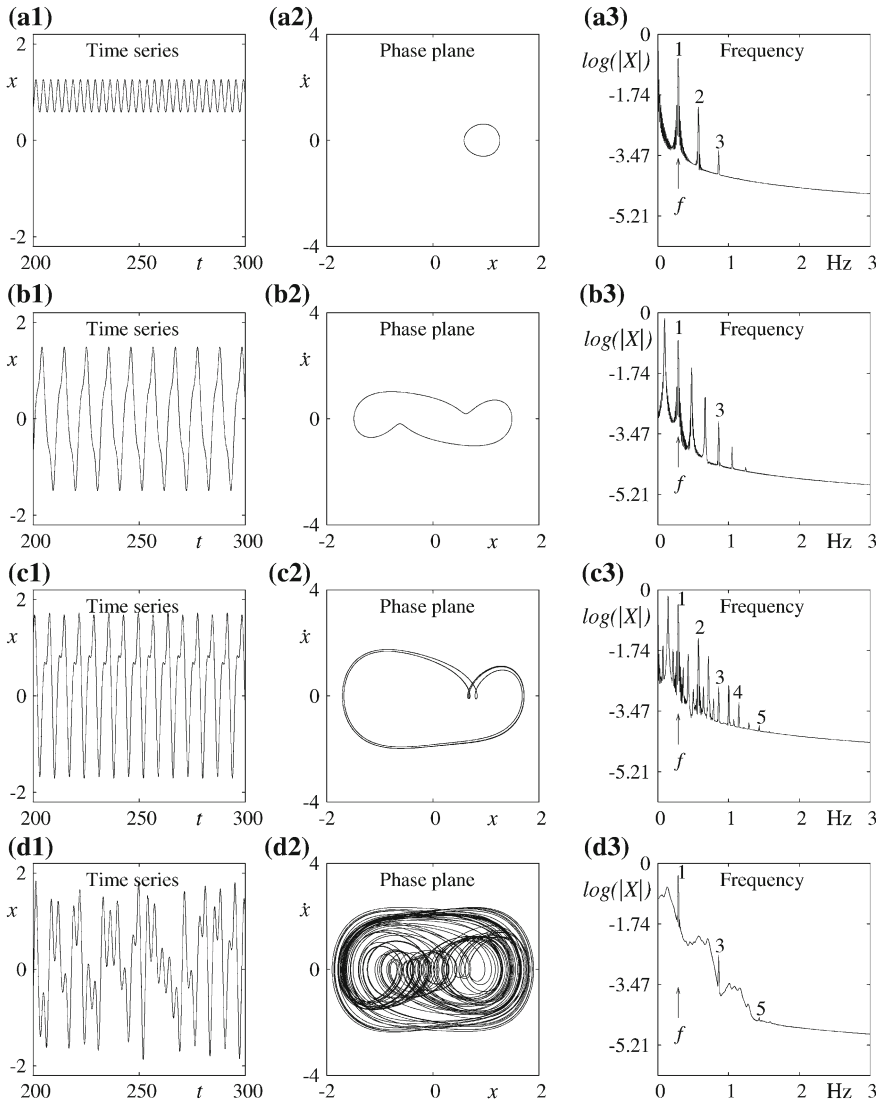


Fig. 2.15 Four different examples of Duffing oscillator dynamics, showing the time series on the left, the phase portrait in the centre and the frequency spectrum on the right

5 are present, as well as a $1/2$ subharmonic and non-integer harmonics at $3/2$, $5/2$, $7/2$ and $9/2$.

Finally, for the case when $F = 1.8$ shown in (d1)–(d3), the response is non-periodic, and in fact in this case is chaotic. Clear evidence for chaotic motion can be seen from the frequency spectrum, which has noticeable peaks at 1, 3 and 5, but is generally much broader in its response compared to the periodic motions. ■

It should be clear from Example 2.6 that (i) in a nonlinear system a range of complex dynamic responses can occur over a relatively short parameter range, and (ii) as a parameter is varied, key changes take place between different dynamic responses. These changes are called *bifurcations* and they are discussed next.

2.6 Parameter Variation and Bifurcations

To investigate the steady-state behaviour of a particular system, one or more of the system parameters can be varied. In vibration engineering, the amplitude and frequency of the external forcing terms are often used to characterize the steady-state system response. As a result, these are natural parameters to vary, but other system parameters may also be used. For linear systems with harmonic forcing, the steady-state response will be made up of one or more resonance peaks, as discussed for example in Chap. 1, Sects. 1.3.1 and 1.3.3.

The stability criterion used so far for linear (or linearized) systems is that an equilibrium point in the upper left-hand quadrant of Fig. 2.6 indicates stability. An alternative way of representing this stability criterion is to plot the system eigenvalues in the complex plane.²⁴ Then for a linear system, if the real parts of the eigenvalues are in the left-hand plane the system is stable, as shown in Fig. 2.16. Conversely, if $\text{Re}(\lambda)$ are in the right-hand plane, the system is unstable. This is because of the exponential form of the solution, given for example in Eq. (2.13). The behaviour follows that shown in Fig. 2.5, in that when the eigenvalue has negative real parts the solution shrinks (Fig. 2.5a), or if the eigenvalue has positive real parts the solution grows exponentially (Fig. 2.5c).

For nonlinear systems, we consider each equilibrium point individually. If for an equilibrium point, the eigenvalues of $D_{\mathbf{x}}*\mathbf{f}$ are in the left-hand plane, then the equilibrium point is locally stable. What happens to the eigenvalues of a stable equilibrium point if a system parameter, μ , is varied? The position of the eigenvalues

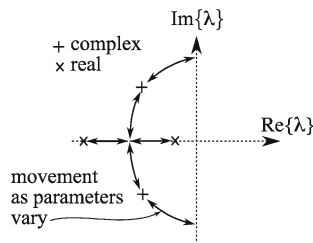


Fig. 2.16 Stable eigenvalues for a linear (or linearized) system showing real, and complex conjugate, cases

²⁴ This is the representation typically used in linear control theory.

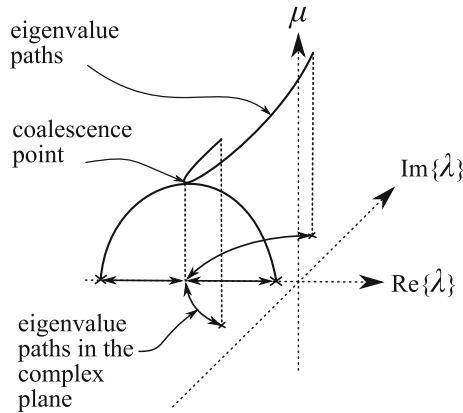


Fig. 2.17 Eigenvalue paths as a parameter is varied

of the linearized system will change,²⁵ as shown in Fig. 2.16 and for a particular value, μ_0 , the real part of one or more of the eigenvalues will become zero. This is when a bifurcation occurs, meaning a substantive change in behaviour—originally a branching point.

In Fig. 2.16 there are two directions in which the stable eigenvalues can change along the paths shown. If the eigenvalues start as a complex conjugate pair and as the parameter changes they reduce in amplitude, they will eventually coalesce on the real axis before diverging as a pair of real eigenvalues. The second case is when the eigenvalues start as real and diverge to become a complex conjugate pair. Figure 2.16 can be replotted to include the parameter being varied, so that the paths of the eigenvalues can be viewed in a three-dimensional space, as shown in Fig. 2.17. A detailed treatment of this type of parameter dependent eigenvalue behaviour is given by Seyranian and Mailybaev (2003).

In terms of the vibration of mechanical, complex eigenvalues indicate underdamped vibration and real eigenvalues overdamped vibration. So in terms of bifurcations, real eigenvalues crossing the imaginary axis tend to relate to *static bifurcations* such as buckling of struts,²⁶ whereas complex eigenvalues crossing the imaginary axis relate to *dynamic bifurcations* such as the sudden appearance of oscillations like flutter.

In fact for equilibrium points in the linear unforced, undamped case, two types of *local* bifurcation have already been discussed. These correspond to the cases of static and dynamic stability loss, as solutions leave the stable upper left quadrant in Fig. 2.6. The dynamic instability corresponds to damping changing sign from positive to negative. In this case the system has complex conjugate eigenvalues, which simultaneously cross the imaginary axis at the point of instability. This type of behaviour is

²⁵ Like a root-locus in linear control theory.

²⁶ Aeroelastic divergence is another example.

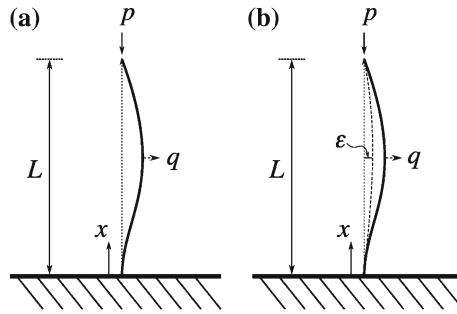


Fig. 2.18 Beam buckling: **a** perfect column, **b** column with eccentricity

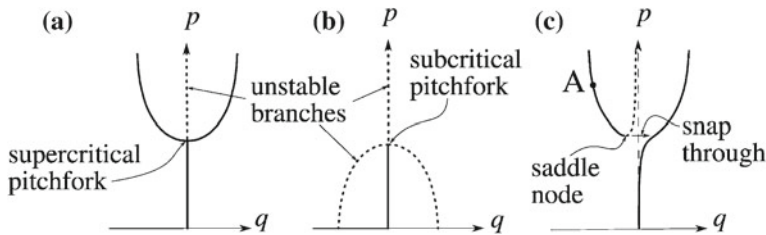


Fig. 2.19 Pitchfork bifurcation: **a** supercritical, **b** subcritical and **c** imperfect

a form of *Hopf bifurcation*²⁷ which will be discussed in greater detail in Sect. 2.6.1. Static instability corresponds to the case when the system has real eigenvalues, and one of the eigenvalues becomes zero at the point when linear stiffness changes sign from positive to negative. This type of bifurcation is characterized by a node changing into a saddle at the point of instability. Depending on the symmetry of the problem, this is either a *saddle-node* bifurcation or a *pitchfork bifurcation*.²⁸

A classic engineering example where both saddle-node and pitchfork bifurcations can be observed is the buckling of an axially-loaded (planar) vertical column, as shown in Fig. 2.18. In Fig. 2.18a a perfectly straight, planar column is loaded with an axial load, p , and the mid-point transverse deflection is q . As the axial load reaches the critical Euler buckling load,²⁹ a pitchfork bifurcation occurs, which is shown in Fig. 2.19a, b. Figure 2.19a is a supercritical pitchfork bifurcation, which corresponds to the physical case when the column adopts a buckled shape but does not collapse. Figure 2.19b is a subcritical pitchfork bifurcation, which corresponds to the physical case when the column fails catastrophically at the point of bifurcation.

²⁷ In fact this is a special case, as there is no limit cycle close to the bifurcation point, see Strogatz (2001).

²⁸ There is a third variation called the *transcritical bifurcation* see Strogatz (2001).

²⁹ See for example Frish-Fay (1962) for details of Euler buckling. For discussions on more complex buckling problems in structural engineering, such as arches and shells, see Thompson and Hunt (1973), Thompson (1982) and Virgin (2007).

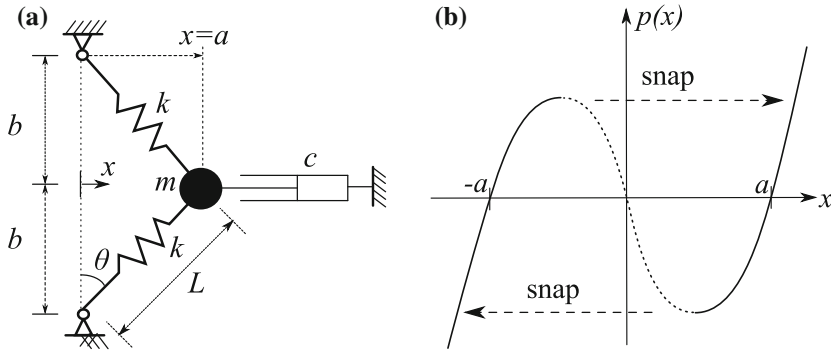


Fig. 2.20 Snap-through system showing, **a** schematic, and **b** nonlinear stiffness function

The two dashed curves linking the bifurcation point to zero correspond to the collapse solutions to the left or right.

In the supercritical case, Fig. 2.19a, after the bifurcation point, the original straight solution becomes unstable (shown as a dashed line) and two stable solutions emerge corresponding to the column buckling either to the left or the right. As the column is perfectly straight, there is an equal chance of the column buckling in either direction. Physically, it is unlikely that the column is perfectly straight, and so the case in Fig. 2.18b is for an imperfect column, where the initial imperfection is represented by the deflection ϵ . The initial imperfection means that the column will always buckle in the same direction. The case for positive ϵ is shown in Fig. 2.19c, where it can be seen that there are now two disconnected solution paths. Increasing p from zero always leads to a buckled shape to the right. If the beam is forced into the opposite (left-hand) buckled shape, and loaded above the Euler load, it can be held in this position, for example at point A in Fig. 2.19c. Physically, the axial load is holding the beam in the buckled state which is opposite to its initial imperfection. Then if the axial load is decreased, at the Euler load the beam will suddenly snap through to the other branch of solutions. The point of snap-through is a saddle-node bifurcation where the stable branch joins an unstable branch that corresponds to the original unbuckled solution.

Notice that in Fig. 2.19 the solid lines indicate the paths of the stable equilibrium points (node/spiral) as p is varied and the dashed lines indicate the unstable equilibrium points (saddles). The unstable and stable branches join at the bifurcation point.

Example 2.7 Bifurcation due to linear stiffness changing sign (Pitchfork)

Problem The physical system shown in Fig. 2.20a has a geometric nonlinearity due to the angle, θ , of the springs. This type of nonlinearity can be approximated by a Duffing-type oscillator with nonlinear stiffness shown in Fig. 2.20b. The equation of motion is given by

$$m\ddot{x} + c\dot{x} - \mu x + \alpha x^3 = 0,$$

where μ and α are coefficients which depend on k , θ and L , the natural length of the springs, and c is viscous damping.³⁰ Assuming $m = 1$ and $\alpha = 1$, find the change in behaviour which occurs as the linear stiffness parameter, μ , is varied and changes sign. What does this change in μ correspond to physically for the system in Fig. 2.20?

Solution First, put the system into first-order form

$$\begin{aligned}\dot{x}_1 &= x_2 = f_1, \\ \dot{x}_2 &= \mu x_1 - x_1^3 - c x_2 = f_2.\end{aligned}$$

By inspection, the equilibrium points for this system are found by equating $f_1 = f_2 = 0$ which gives

$$\begin{array}{llll}\mu < 0 & x_1 = 0 & x_2 = 0, & \text{one equilibrium point} \\ \mu = 0 & x_1 = 0 & x_2 = 0, & \text{one equilibrium point} \\ \mu > 0 & x_1 = 0 & x_2 = 0, & \\ \text{and} & x_1 = \pm\sqrt{\mu} & x_2 = 0, & \text{three equilibrium points.}\end{array}$$

To investigate the behaviour, the system is linearized locally close to the equilibrium points. For all μ values the equilibrium point $\mathbf{x}_a^* = (x_1 = 0, x_2 = 0)$ exists. For $\mu > 0$ values, two additional equilibrium points exist and are labelled as $\mathbf{x}_{b,c}^* = (x_1 = \pm\sqrt{\mu}, x_2 = 0)$. In general, the Jacobian for the system is

$$D_{\mathbf{x}}\mathbf{f} = \frac{\partial(f_1, f_2)}{\partial(x_1, x_2)} = \begin{bmatrix} \frac{\partial f_1}{\partial x_1} & \frac{\partial f_1}{\partial x_2} \\ \frac{\partial f_2}{\partial x_1} & \frac{\partial f_2}{\partial x_2} \end{bmatrix} = \begin{bmatrix} 0 & 1 \\ \mu - 3x_1^2 & -c \end{bmatrix}.$$

First for $\mathbf{x}_a^* = (x_1 = 0, x_2 = 0)$, the Jacobian becomes

$$D_{\mathbf{x}_a^*}\mathbf{f} = \begin{bmatrix} 0 & 1 \\ \mu & -c \end{bmatrix}.$$

So for equilibrium point \mathbf{x}_a^* , $\text{tr}(A) = -c$ and $\det(A) = -\mu$.

For equilibrium points $\mathbf{x}_{b,c}^* = (x_1 = \pm\sqrt{\mu}, x_2 = 0)$, the Jacobian becomes

$$D_{\mathbf{x}_a^*}\mathbf{f} = \begin{bmatrix} 0 & 1 \\ -2\mu & -c \end{bmatrix}.$$

So in this case $\text{tr}(A) = -c$ and $\det(A) = 2\mu$.

³⁰ The derivation of a Duffing oscillator from the snap-through system can be found as the solution to Problem 2.1. Note that the mass is at static equilibrium when $x = \pm a$, and the springs are at their natural length, L .

Note that the expression for $\text{tr}(A)$ and $\det(A)$ are computed assuming that $\mu > 0$. In the case when $\mu < 0$ the sign of μ terms *will change*. So for equilibrium point \mathbf{x}_a^* (using Fig. 2.6) when

$$\begin{array}{ll} \mu < 0, & \text{tr}(A) = -c, \det(A) = -(-\mu) = \mu, \quad \text{stable node/spiral} \\ \mu = 0, & \text{tr}(A) = -c, \det(A) = 0, \quad \text{degenerate case} \\ \mu > 0, & \text{tr}(A) = -c, \det(A) = -\mu, \quad \text{saddle} \end{array}$$

so this equilibrium point changes from a stable node/spiral to a saddle point as μ passes through zero. In general, for $\mu > 0$ the discriminant is $\Delta = \text{tr}^2 - 4\det = c^2 + 4\mu$. So the μ value at which $\Delta = 0$ is $\mu = -c^2/4$, marking the degenerate node case from Fig. 2.6. So for $-c^2/4 < \mu < 0$, \mathbf{x}_a^* is a stable node and for $\mu < -c^2/4$ a stable spiral.

For equilibrium points $\mathbf{x}_{b,c}^*$ when

$$\begin{array}{ll} \mu < 0, & \text{n/a,} \quad \text{no equilibrium point} \\ \mu = 0, & \text{tr}(A) = -c, \det(A) = 0, \quad \text{degenerate case} \\ \mu > 0, & \text{tr}(A) = -c, \det(A) = 2\mu, \quad \text{stable node/spiral} \end{array}$$

So, for $\mu < 0$, there are no equilibrium points. For \mathbf{x}_b^* , c the discriminant is $\Delta = \text{tr}^2 - 4\det = c^2 - 8\mu$. So the μ value at which $\Delta = 0$ is $\mu = 1/8$, marking the degenerate node case from Fig. 2.6. So for $0 < \mu < c^2/8$, $\mathbf{x}_{b,c}^*$ are stable nodes and for $\mu > c^2/8$ they become a stable spirals.

Physically changing μ from negative to positive corresponds to the system in Fig. 2.20 having positive linear stiffness. Geometrically, this can be considered in terms of the length of the springs. So, in the case when $b < L$ the springs are in compression and $\mu < 0$. Conversely, when $b > L$ the springs are in tension and $\mu > 0$. ■

The physical interpretation of the snap-through can be seen from Fig. 2.21, where in (a1) and (a2) the linear stiffness is negative, (b1) and (b2) shows the $\mu = 0$ case and (c1) and (c2) shows the case where the linear stiffness is positive. This corresponds to moving the end supports apart from (a1)–(b1) and finally (c1). In (b1) there is no tension or compression in the springs, whereas in (c1) the springs are in tension.

This type of transition is known as a *cusp bifurcation*, because if plots (a2), (b2) and (c2) are combined into a surface plot with μ as the additional coordinate, then the surface has a cusp at $\mu = 0$. See Thompson (1982) for further details of this phenomenon.

From a mechanical vibration perspective, bifurcations of equilibria relate primarily to unforced systems and/or static stability. A more significant class of bifurcations for vibration analysis are those that lead to oscillations. These are considered next.

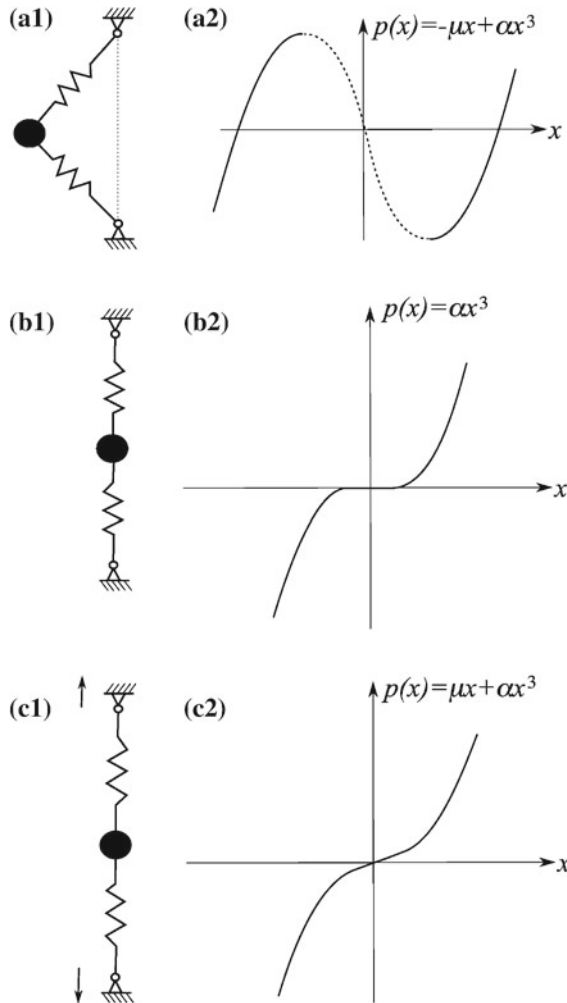


Fig. 2.21 Change in stiffness function as μ varies for Example 2.7

2.6.1 The Onset of Oscillations via a Hopf Bifurcation

This subsection describes an important phenomenon that occurs in nonlinear vibrations. It occurs when a stable equilibrium point becomes unstable and is replaced by a limit cycle as a parameter is varied. The point at which this happens is called a Hopf bifurcation. Numerous physical examples of this type of phenomenon exist. In engineering, Hopf bifurcations are often associated with systems where fluid flow is the external forcing, and the flow speed is the parameter which triggers the bifurcation. A simple example is fluid flowing through a hose pipe at slow speeds does not

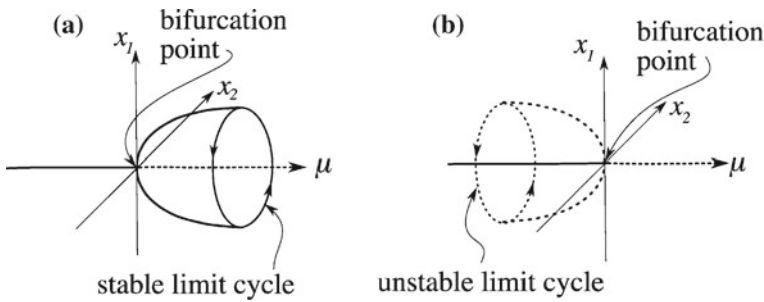


Fig. 2.22 Hopf bifurcation: **a** supercritical, **b** subcritical

induce any (large) oscillations in the pipe. As the flow speed is increased, there comes a critical point where large oscillations in the pipe occur due to a Hopf bifurcation (try an experiment with your garden hose).

A significant physical example is flutter in aeroelastic vibration problems. This is a major design consideration for aerospace structures. Other examples include oscillations in cables immersed in a fluid flow, for example on bridges, and the onset of lateral oscillations in train carriages at a critical speed.

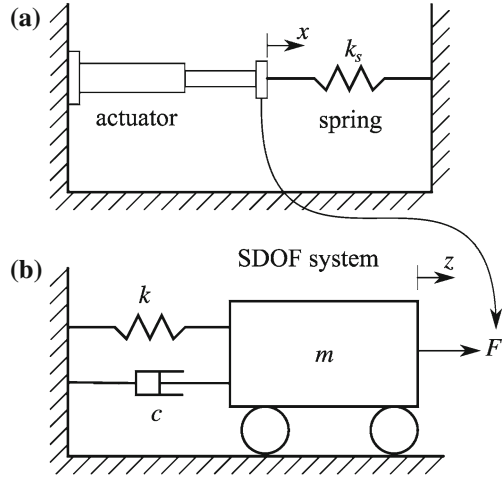
A schematic representation of the two different types of Hopf bifurcation is shown in Fig. 2.22. As the system parameter, μ , is varied, a stable equilibrium point at the origin ($x_1 = 0$, $x_2 = 0$) goes unstable at the bifurcation point, $\mu = 0$. There are two cases (like the pitchfork), in the supercritical case (Fig. 2.22a) a stable limit cycle exists for $\mu > 0$. In the subcritical case (Fig. 2.22b) no stable limit cycle exists for $\mu > 0$, instead an unstable limit cycle exists for $\mu < 0$. As a result the subcritical case can be viewed as potentially catastrophic, because after the bifurcation the system has no (local) stable solution to stabilize onto. Instead, if there are no solutions nearby, the system could jump to a distant solution or escape to infinity. Determining whether a particular bifurcation is super- or sub-critical can be done by either numerical simulation or using *centre manifold theory*. This is a major topic of dynamical systems theory, and good introductions are given by Guckenheimer and Holmes (1983), Thompson and Stewart (2002), Glendinning (1994) and Strogatz (2001).

Another important class of systems in which Hopf bifurcations occur are those with delays. This is especially important when applying control to dynamic systems, as actuators can introduce delays into the overall system. An example is considered next.

Example 2.8 Hopf bifurcation due to actuator delay

Problem An experimental test is configured such that an actuator is attached to a linear spring, k_s , as shown in Fig. 2.23. The actuator is controlled to follow (track) the output, z , of a single-degree-of-freedom mass-spring oscillator (m , c , k) system and the force from the actuator, F , is fed into the single degree of freedom—see Chap. 7 of Bursi and Wagg (2008) for a complete description of this system. Assuming perfect control tracking, underdamped vibrations, and that the actuator dynamics

Fig. 2.23 Schematic representation of the experimental test system. See Chap. 7 of Bursi and Wagg (2008) for a complete description of this system



can be modelled as a small fixed delay, τ , find the eigenvalues of the system and use them to examine the stability of the equilibrium point at the origin in terms of the parameter τ .

Solution The governing equation of the single-degree-of-freedom system is

$$m\ddot{z} + c\dot{z} + kz = F,$$

where the feedback force $F = -k_s x$ and x is the actuator displacement (from Fig. 2.23a). For perfect control tracking $x = z$, but the key observation is that the actuator introduces a delay such that $x(t) = z(t - \tau)$, $\tau > 0$. The overall system is then governed by the delay differential equation³¹

$$m\ddot{z} + c\dot{z} + kz + k_s z(t - \tau) = 0. \quad (2.29)$$

The characteristic equation can be found by assuming solutions of the form $z(t) = Ce^{\lambda t}$, where C is an arbitrary constant, which for the delay term gives $z(t - \tau) = Ce^{\lambda(t - \tau)}$. Substituting these expressions into Eq. (2.29) gives

$$m\lambda^2 + c\lambda + k + k_s e^{-\lambda\tau} = 0,$$

because $e^{\lambda(t - \tau)} = e^{\lambda t} e^{-\lambda\tau}$ so that the $Ce^{\lambda t}$ factors can be divided out, leaving just the $e^{-\lambda\tau}$ exponential term.³²

³¹ The introduction of a fixed delay means that the delay differential equation actually has an infinite-dimensional state space, see Stépan (1989) or Diekmann et al. (1995) for an introduction to delay differential equations.

³² In fact, this is an infinite-dimensional eigenvalue problem. However, only two are significant in this case. See Stépan (1989) or Diekmann et al. (1995) for further details.

If the delay, τ , is small, then the approximation $e^{-\lambda \tau} \approx (1 - \lambda \tau)$ can be made, which gives

$$m\lambda^2 + c\lambda + k + k_s(1 - \lambda \tau) \rightsquigarrow m\lambda^2 + \lambda(c - k_s \tau) + k + k_s \approx 0. \quad (2.30)$$

The solution of Eq. (2.30) is

$$\lambda_{1,2} = \frac{1}{2m} \left[(k_s \tau - c) \pm \sqrt{(c - k_s \tau)^2 - 4m(k + k_s)} \right].$$

For underdamped vibrations and τ small, physically realistic parameters result in complex eigenvalues. Or, in other words, assume that $4m(k + k_s) > (c - k_s \tau)^2$ for all realistic choices of m, c, k, k_s and τ . Then the stability of the eigenvalues is governed by the real part, specifically by the sign of $(k_s \tau - c)$. If $(k_s \tau - c) < 0$ the eigenvalues are complex and stable. When $(k_s \tau - c) > 0$ the eigenvalues are unstable. The transition occurs when $(k_s \tau - c) = 0$ or $\tau = \frac{c}{k_s}$. The value of τ at which the transition occurs corresponds to complex eigenvalues crossing the imaginary axis from left to right, which is a Hopf bifurcation.

Physically, the delay can be interpreted as negative damping, with an equivalent negative damping term of $c_{neg} = -k_s \tau$. ■

2.6.2 Bifurcations in Forced Nonlinear Oscillations

When a (damped) nonlinear system is forced, one of the most likely steady-state responses is a limit cycle (also called periodic orbit) type of behaviour. Note that when the system has more than one degree-of-freedom, limit cycles typically exist for each degree-of-freedom (or mode of vibration, discussed further in Chap. 5). Examining the response behaviour as a parameter varies allows a comprehensive picture to be built up of the system dynamics. In the linear single- and multi-degree-of-freedom systems (for example, those discussed in Chap. 1, Sects. 1.3.1 and 1.3.3), varying the forcing frequency leads to changes in limit cycle amplitude, but no changes to the *structure*, of the limit cycle occurs. For nonlinear systems, the limit cycle structure can change and the points at which this happens are bifurcation points.

To analyse bifurcations of limit cycles, the cycle is typically linearized in some local region of state space. A way to linearize a limit cycle is to use the stroboscopic map. For a steady-state vibration in the form of a limit cycle, the stroboscopic map is formed by *sampling* the cycle once per forcing period. For example, if T is the forcing period, then at times $t = 0, T, 2T, 3T, \dots$ the values of displacement d_n and velocity v_n are recorded, to get a series of data points $(d_0, v_0), (d_1, v_1), (d_2, v_2), (d_3, v_3), \dots$, corresponding to the sampling times. For example in Fig. 2.24a two planes a distance T apart are shown intersecting with the trajectory, L . In the first plane at $t = 0$ the path of L intersects the plane at

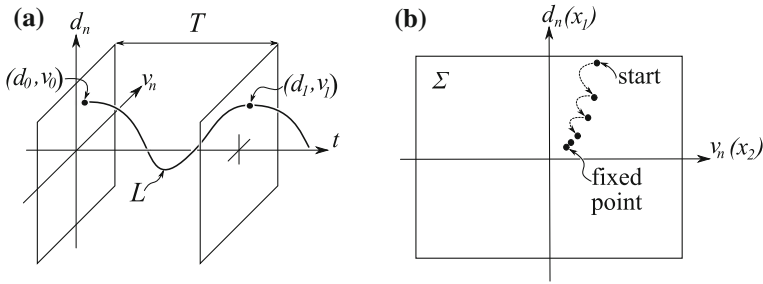


Fig. 2.24 The stroboscopic map, showing **a** the continuous orbit in d_n, v_n, t space, and **b** and example of a transient motion, showing the *points* that the orbit makes in the d_n, v_n plane. Notice that as the transient motion decays and the system becomes a steady state limit cycle, the *points* move towards a fixed point in the plane

point (d_0, v_0) (the initial conditions) and at time $t = T$ the intersection is at point (d_1, v_1) . Plotting all these points on top of each other in a single displacement-velocity plane, denoted Σ , shows the evolution of the trajectory towards its final steady state behaviour, which in this case is a limit cycle. An example of the Σ plane is shown in Fig. 2.24b. This shows a series of transient points in the plane, sampled at $t = 0, T, 2T, 3T, \dots$, converging towards a *fixed point*³³ in the plane Σ .

Now, the fixed point in the map corresponds to the limit cycle in the *flow*, where flow is the evolution of multiple nearby, continuous time, trajectories in state space. So if the mapping can be linearized close to the fixed point, the eigenvalues³⁴ of the linearized system will indicate the type of fixed point behaviour and where bifurcations occur.

The state vector for the mapping is written in a discrete time formulation as $\mathbf{x}_n = [d_n, v_n]$, and the general nonlinear relationship is $\mathbf{x}_{n+1} = \mathbf{h}(\mathbf{x}_n)$, where each n in the map corresponds to a forcing period in the continuous time oscillator. A fixed point in the map³⁵ is denoted \mathbf{x}^* , and has the property that $\mathbf{x}^* = \mathbf{h}(\mathbf{x}^*)$. Linearising the mapping close to the fixed point means first defining a new coordinate with an origin at the fixed point $\xi_n = \mathbf{x}_n - \mathbf{x}^*$. Then $\xi_{n+1} = \mathbf{x}_{n+1} - \mathbf{x}^* = \mathbf{h}(\mathbf{x}_n) - \mathbf{x}^*$ or $\xi_{n+1} = \mathbf{h}(\mathbf{x}^* + \xi_n) - \mathbf{x}^*$. Taking a Taylor expansion of the nonlinear mapping function, $\mathbf{h}(\mathbf{x}^* + \xi_n)$, gives the approximation

$$\xi_{n+1} \approx \mathbf{h}(\mathbf{x}^*) + D_{\mathbf{x}^*} \mathbf{h} \xi_n + \mathcal{O}(\|\xi_n\|^2) - \mathbf{x}^*,$$

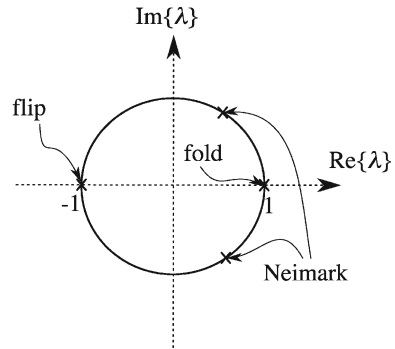
where the notation $D_{\mathbf{x}^*}$ is the same as that used for computing the Jacobian in Eq. (2.11). Now it can be seen that because $\mathbf{h}(\mathbf{x}^*) = \mathbf{x}^*$, the expression for ξ_{n+1} reduces to

³³ A fixed point in a map can be thought of as analogous to equilibrium point in a continuous flow.

³⁴ Also sometimes referred to as the Floquet multipliers of the periodic orbit.

³⁵ This definition is for the lowest order return period i.e. one. Higher order periodicity maps can be defined, and the interested reader can find details in Thompson and Stewart (2002).

Fig. 2.25 Eigenvalues of a linearized mapping



$$\xi_{n+1} \approx D_{\mathbf{x}^*} \mathbf{h} \xi_n + \mathcal{O}(\|\xi_n\|^2).$$

For mappings, the stability criterion for eigenvalues in the complex plane is different from that for equilibria. Now, any eigenvalue with a modulus greater than one³⁶ will lead to instability. This is shown in Fig. 2.25. There are three ways in which stability can be lost. For an eigenvalue of $\lambda = 1$ the system undergoes a cyclic saddle-node or *fold* bifurcation. For an eigenvalue of $\lambda = -1$ the system undergoes a *flip* bifurcation (also known as a *period-doubling* bifurcation). For a complex eigenvalue with $|\lambda| = 1$, the system undergoes a secondary Hopf or *Neimark-Sacker* bifurcation.

Example 2.9 Fixed points in the Henón map³⁷

Problem The Henón map is a two state mapping which can be represented as

$$\begin{aligned} x_{n+1} &= 1 - ax_n^2 + y_n, \\ y_{n+1} &= bx_n, \end{aligned}$$

where x_n, y_n are the system states, and a, b are parameters. Determine the condition for the fixed points of the system to be real. Then compute the stability of the fixed point which exists at values of $a = -\frac{1}{16}$ and $b = \frac{1}{2}$. Comment on the eigenvalues of this fixed point in terms of the expected bifurcation behaviour of the system.

Solution First we write the map as

$$\begin{aligned} x_{n+1} &= 1 - ax_n^2 + y_n = h_1, \\ y_{n+1} &= bx_n = h_2. \end{aligned}$$

³⁶ In discrete systems λ act as multipliers, so $|\lambda| > 1$, solution grows, unstable; $|\lambda| < 1$, solution shrinks, stable.

³⁷ See Thompson and Stewart (2002) for details of the derivation of this and other maps.

For a fixed point of the map x_n^*, y_n^* we have by definition

$$\begin{aligned} x_n^* &= h_1(x_n^*, y_n^*) = 1 - ax_n^{*2} + y_n^*, \\ y_n^* &= h_2(x_n^*, y_n^*) = bx_n^* \end{aligned} \quad (2.31)$$

and by substituting the second of these expressions into the first we obtain

$$x_n^* = 1 - ax_n^{*2} + bx_n^*, \quad \rightsquigarrow \quad ax_n^{*2} + (1 - b)x_n^* - 1 = 0$$

from which it can be determined that the solutions are given by

$$x_{n:1,2}^* = \frac{(1 - b) \pm \sqrt{(1 - b)^2 - 4a(-1)}}{2a}. \quad (2.32)$$

As a result, the condition for real solutions is the same as ensuring that the discriminant is greater than or equal to zero, such that

$$(1 - b)^2 - 4a(-1) \geq 0 \quad \rightsquigarrow \quad (1 - b)^2 + 4a \geq 0 \quad \rightsquigarrow \quad a \geq -\frac{1}{4}(1 - b)^2.$$

When $a = -\frac{1}{16}$ and $b = \frac{1}{2}$ the discriminant is zero, so this will lead to a real fixed point(s). Substituting these values into Eq. 2.32 gives $x_n = 4$, and then from Eq. 2.31 it is found that $y_n = 2$.

The Jacobian of the map is given by

$$D_{\mathbf{x}}\mathbf{h} = \frac{\partial(h_1, h_2)}{\partial(x_n, y_n)} = \begin{bmatrix} \frac{\partial h_1}{\partial x_n} & \frac{\partial h_1}{\partial y_n} \\ \frac{\partial h_2}{\partial x_n} & \frac{\partial h_2}{\partial y_n} \end{bmatrix} = \begin{bmatrix} -2ax_n & 1 \\ b & 0 \end{bmatrix}.$$

Now to evaluate the stability of the fixed point at $x_n = 4$, $y_n = 2$, we substitute these values into the Jacobian to obtain

$$D_{\mathbf{x}^*}\mathbf{h} = \begin{bmatrix} -2(-\frac{1}{16})4 & 1 \\ \frac{1}{2} & 0 \end{bmatrix} = \begin{bmatrix} \frac{1}{2} & 1 \\ \frac{1}{2} & 0 \end{bmatrix}.$$

The eigenvalues of this Jacobian matrix are $\lambda_1 = 1$ and $\lambda_2 = -\frac{1}{2}$. An eigenvalue of +1 means that the system is on the boundary of stability (as shown in Fig. 2.25), and the system is undergoing a fold bifurcation. ■

A set of numerically computed data of the Henón map is shown in Fig. 2.26. First in Fig. 2.26a a *chaotic attractor*³⁸ which occurs for the parameter values $b = 0.3$ and

³⁸ We will not give further detailed discussion on chaos, but a good references are the books by Guckenheimer and Holmes (1983), Moon (1987), Glendinning (1994), Strogatz (2001) and Thompson and Stewart (2002).

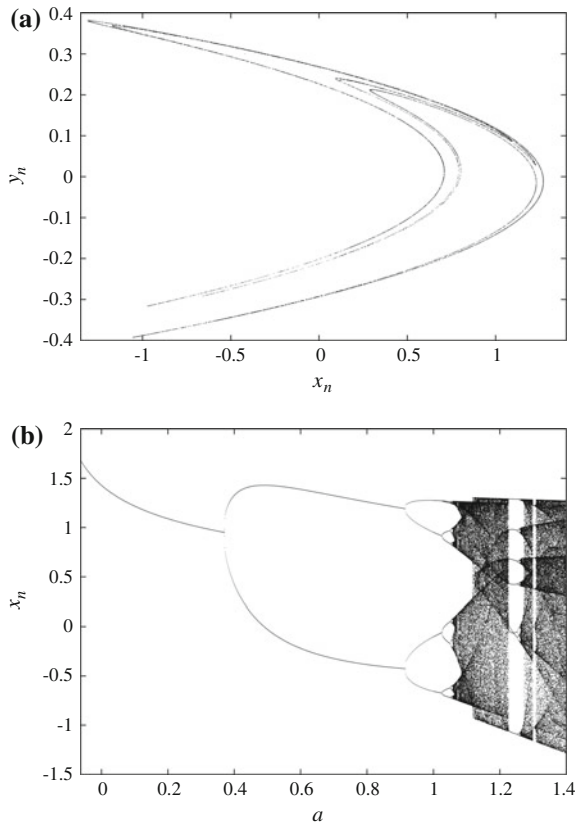


Fig. 2.26 Hénon map, showing **a** the chaotic attractor at $b = 0.3$ and $a = 1.42$, **b** a bifurcation diagram as a is varied

$a = 1.42$ is shown. For maps, a stable limit cycle is a fixed point attractor because nearby transient points are attracted towards it (as shown in Fig. 2.24b). Chaotic attractors act in the same way, in that nearby transient points are drawn onto the attractor.

In Fig. 2.26b, the value of x_n is shown as the parameter a is varied. This is called a bifurcation diagram. Starting on the extreme left of the diagram the system is at the fold bifurcation discussed in Example 2.9. Then for $-0.0625 < a < 0.4$ (approx) there is just one x_n value for each a value, so this is a period one behaviour. At approximately $a = 0.4$ (for increasing a), a flip (period doubling) bifurcation occurs, so now there are two x_n values for each a . This happens again at approx $a = 0.93$ and so then 4 x_n values occur. After $a \approx 1.1$ there is a rapid transition into chaotic motion, via a period doubling cascade. Note that the chaotic region has some narrow windows of periodic behaviour within it.

Now consider what happens when the period of the limit cycle changes from one forcing period to two forcing periods. This scenario is shown in Fig. 2.27, where a

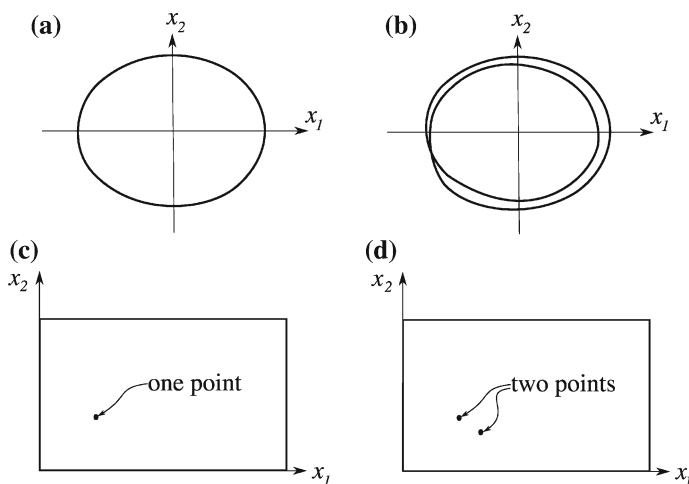


Fig. 2.27 Period-doubling (flip) bifurcation: **a** before, **b** after, **c** map before and **d** map after

period-1 limit cycle in (a) becomes a period-2 orbit in (b). Schematic representations of the stroboscopic maps³⁹ are shown in Fig. 2.27c, d, where there is a change from 1 to 2 points in the map.

In practice, it is very rarely possible to write down the mapping explicitly for the majority of nonlinear vibration problems. As a result, investigating a particular system is usually done by computing the map numerically. Numerical estimations of the Jacobian can be found, for example, by using finite differences—see Foale and Thompson (1991) for a description of numerical investigations of these types of systems. The numerical results are then usually plotted as a series of *bifurcation diagrams*. Typically, for vibration problems, the bifurcation parameters of interest will be the forcing amplitude and frequency, so the bifurcation diagrams will be closely linked to the frequency and amplitude response plots used for linear vibration studies.

One way to obtain a bifurcation diagram is to compute a time series of the system, allowing a large enough number of forcing periods to decay such that steady-state behaviour has been reached. Then plot the amplitude of one of the system states (usually displacement) for a number of steady state periods, before incrementing the parameter by a small amount and repeating. Note that it is important *not* to reset the initial conditions after each parameter increment. In other words, keep the last x_n and t values from the steady-state, to use as the initial conditions after the parameter has been incremented. This is how the bifurcation diagram was computed for the Henón map shown in Fig. 2.26b. The idea is to observe how a particular solution changes its behaviour as a parameter is varied (for example the parameter a in Fig. 2.26b). Once the maximum parameter value of interest is reached, the process should be repeated

³⁹ Note that in general these types of maps are called *Poincaré* maps, see Strogatz (2001).

for decreasing parameter values through the full range, back to the starting value. This will allow any regions of *hysteresis* to be captured. Also, multiple steady-state points (usually at least ten or more) are plotted for each parameter value, in order to capture any multi-periodic or chaotic behaviour.

The approach described here is one of the most basic, and is sometimes referred to as the *brute-force* approach. It is useful for a quick and approximate assessment of the system, but care is needed, as problems can arise. Of course bifurcation theory is a highly developed field in its own right (see for example Guckenheimer and Holmes 1983; Kuznetsov 2004) and there is a range of sophisticated associated numerical techniques (see for example Doedel et al. 1998; Krauskopf et al. 2007), which make it possible to start from a fixed point and then *continue* the path of the fixed point, in state space, as a parameter is varied. Where brute force will normally only capture stable steady-state solutions,⁴⁰ continuation methods can be used to capture both stable and unstable branches, as shown in Fig. 2.28 which is discussed next.

Bifurcations of limit cycles lead to structural changes in the resonance behaviour of nonlinear oscillators. One of the most common examples is shown in Fig. 2.28. This resonance peak has been simulated from a Duffing oscillator (similar to Example 2.6), using the brute-force method described above. The parameter varied is the ratio of the forcing frequency to the (linear) natural frequency of the oscillator, $\mu = \Omega/\omega_n$. The measurement taken, for each frequency value, is the maximum displacement per forcing period. The resulting bifurcation curve is then the envelope function defining the resonance amplitude of the oscillator. This is similar to the linear dynamic amplification function for a linear system plotted in Chap. 1, Fig. 1.10.

The resonance peak in Fig. 2.28 is distorted (or bent) to the right, and contains two fold bifurcations, on either side of a region of hysteresis. In this context, hysteresis means that a different behaviour is obtained for increasing or decreasing ω . As ω is increased, a stable solution path gradually increases in amplitude until it reaches fold *A*. Here, the stable path joins an unstable path of solutions. If ω is increased beyond the bifurcation point, there is a jump to the lower stable branch. When decreasing ω from above the resonance, the stable path continues until fold *B*, where there is a jump up to the upper stable branch. The region between fold *A* and *B* is the region of hysteresis.

This type of resonance is associated with a *hardening* spring nonlinearity, meaning a spring which becomes stiffer as it displaces further. The opposite case is a softening spring, meaning a spring that becomes *less* stiff as it displaces further. This leads to a resonance peak that bends to the left, as shown in Fig. 2.29a.

In Fig. 2.29b a double fold behaviour is shown. This is in fact also for the Duffing oscillator, but instead of using forcing frequency, Ω , as the bifurcation parameter, in this example the forcing amplitude, F , is varied, with Ω selected within the hysteresis region.

Finally, note that the discussion in this section has been for *local* bifurcations. Global bifurcations are significant changes in dynamics which happen when struc-

⁴⁰ Running time backwards reverses the stability of solution branches, so in this way brute force can be used in some cases to find unstable solutions like repellers, but not saddles.

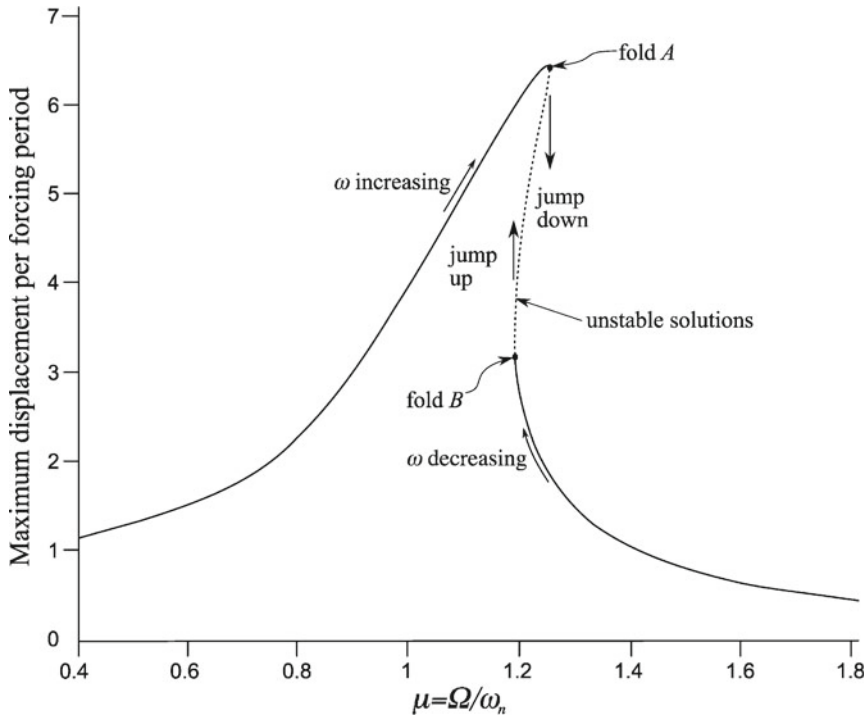


Fig. 2.28 Nonlinear resonance with hysteresis for the Duffing oscillator $\ddot{x} + \zeta \omega_n \dot{x} + \omega_n x + \alpha x^3 = F \cos(\Omega t)$ with a hardening spring $\alpha > 0$

tures in the phase plane, like equilibrium/fixed points, limit cycles come together as a parameter is varied. One such case has already been mentioned in the discussion of Example 2.4, where the limit cycle grows in size until it touches the saddle equilibrium point resulting in a homoclinic bifurcation. Discussions on global bifurcations can be found in Guckenheimer and Holmes (1983) and Glendinning (1994).

2.7 Systems with Harsh Nonlinearities

So far in this chapter little has been said about how *strong* or *severe* the nonlinearity in any particular vibrating system might be. In fact, most of the systems discussed in this chapter have relatively *weak* nonlinear terms. In Chap. 1, Sect. 1.2.4 some examples of what can collectively be called *harsh* nonlinearity were introduced. In this context, harsh means the most severe type of nonlinearity. This is characterised by sudden, and large changes in parameters. Common examples include; impact, friction, freeplay and backlash phenomena. In this section we will briefly discuss two important examples, the *friction oscillator* and the *impact oscillator*.

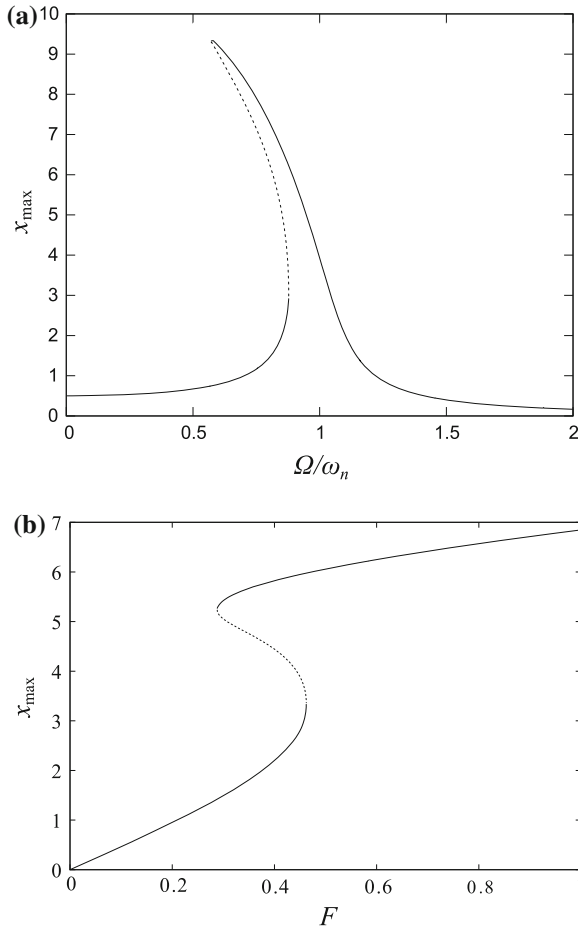


Fig. 2.29 Examples of bifurcation behaviour for the Duffing oscillator $\ddot{x} + \zeta\omega_n\dot{x} + \omega_n x + \alpha x^3 = F \cos(\Omega t)$ with, **a** a softening spring $\alpha < 0$ showing the resonance peak bending to the *left*, and **b** double fold also for the Duffing oscillator, but using forcing amplitude, F , as the bifurcation parameter

2.7.1 Friction Oscillator

One of the most difficult to model nonlinear vibration phenomena is when a dynamic system involves friction. It is also a phenomena that is widely exploited in engineering applications to damp out vibration and provide braking mechanisms (Guran et al. 1996; Sextro 2002). There are many models for friction, and three such models are shown schematically in Fig. 2.30. The models shown in Fig. 2.30 are defined in terms of the friction force, F , against a velocity, v , which is typically taken to be the velocity of a moving mass at the friction interface. Both Fig. 2.30a, b show very strong changes in friction force in the vicinity of $v = 0$, which represents the

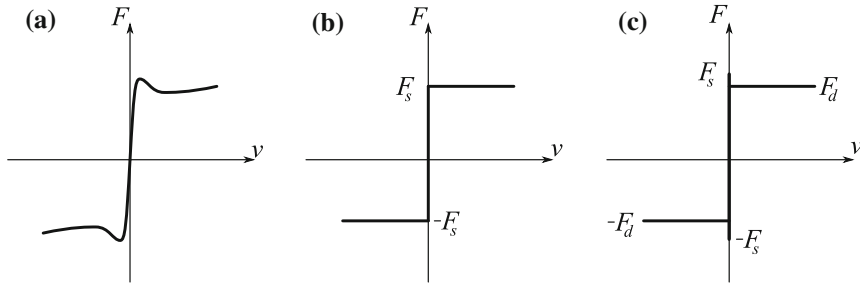


Fig. 2.30 Models for friction force, F , showing **a** continuous, **b** simple Coulomb, and **c** modified Coulomb

behaviour observed from physical systems. The main difference is that Fig. 2.28a is a continuous function curve while Fig. 2.30b is a *non-smooth* function. The continuous model is more representative of the physics involved,⁴¹ but when implementing it as a dynamic model, the complex continuous function is normally approximated. The model in Fig. 2.30b is considerably easier to implement, but the key difference between static and dynamic friction is not captured. This limitation can be partly overcome by using the model in Fig. 2.30c which has been modified to include both the static friction, F_s , and dynamic (or sliding) friction F_d . Depending on the context, models of the type shown in Fig. 2.30b, c are referred to as the Coulomb friction model.

The Coulomb model can be represented mathematically as

$$F_{Coulomb} = \begin{cases} +F_d, & v > 0 \\ -F_s < F < F_s, & v = 0 \\ -F_d, & v < 0 \end{cases}$$

where F_s is the static friction force, often defined for simple friction models as $F_s = \mu N$ where μ is the coefficient of friction and N is the normal force at the frictional interface.⁴²

Example 2.10 The friction oscillator

Problem A lumped mass oscillator system with friction is shown schematically in Fig. 2.31a. This is a single degree-of-freedom spring-mass-damper system where the mass, m , is resting on a taut belt rotating at a constant velocity, V . This oscillator system is known as a *friction oscillator*, and can be represented by a governing equation of the form

⁴¹ For example it can capture the down then upward curving trend for $|v|$ increasing, known as the Stribeck effect.

⁴² Note that this definition relies on Amonton's laws of friction. i.e. that the friction force is directly proportional to the normal load and independent of area. This will restrict the situations in which it could be applied in practice.

$$m\ddot{x} + c\dot{x} + kx + F_f = 0$$

where F_f is the friction force between the mass, m , and the belt. This oscillator equation is combined with the Coulomb model, such that $F_f = F_{Coulomb}$, to give a complete model of the system. Using numerical techniques find one characteristic behaviour of the system when $m = 2 \text{ kg}$, $k = 10 \text{ N/m}$, $F_s = 9.81 \text{ N}$, $F_d = 5.89 \text{ N}$, $V = 0.2 \text{ m/s}$, and $c = 0$.

Solution The friction oscillator can exhibit a range of dynamic behaviour, and for the parameters given in this problem the resulting numerically computed result is shown in Fig. 2.31b. This is known as a *stick-slip* oscillation. In this type of oscillation the mass is stuck to the belt for part of the period, which is represented by the horizontal line of constant velocity $v = V = 0.2$. As x increases the restoring force due to the spring grows, until at the top right hand point of the cycle it overcomes the static friction force and the mass starts to move. This happens repeatedly in a periodic motion due to the difference between the spring force and the dynamic friction force at the onset of slip. Note that as we have used a non-smooth friction law, the periodic cycle is also non-smooth. Other motions are possible, such as constant slipping and chaotic motion.

2.7.2 Impact Oscillator

The combined effect of vibration with impacting components is a harsh nonlinearity encountered in a wide range of engineering applications. For example consider a ball experiencing an impact with a wall as shown schematically in Fig. 2.32a. As the ball impacts the wall there is a process of compression followed by restitution,⁴³ as shown in Fig. 2.32b. If no energy is lost (not possible in practice) the restitution phase will be exactly symmetric with the compression phase. However, in practice, some energy is always lost during impact and this is seen by the fact that the velocity of the ball after impact is both reversed and reduced, compared to the velocity before impact. This is shown in Fig. 2.32c.

This change and reduction in velocity can be captured by a simple model called the coefficient of restitution⁴⁴ law

$$\dot{x}(t_e) = -r\dot{x}(t_s) \quad (2.33)$$

⁴³ Note both the ball and the wall will deflect. How much depends on the material and geometric properties.

⁴⁴ Also referred to as the Newtonian coefficient of restitution, this type of impact model assumes that there is no tangential force during the impact. See Stronge (2000) for details of this and other more complex impact cases.

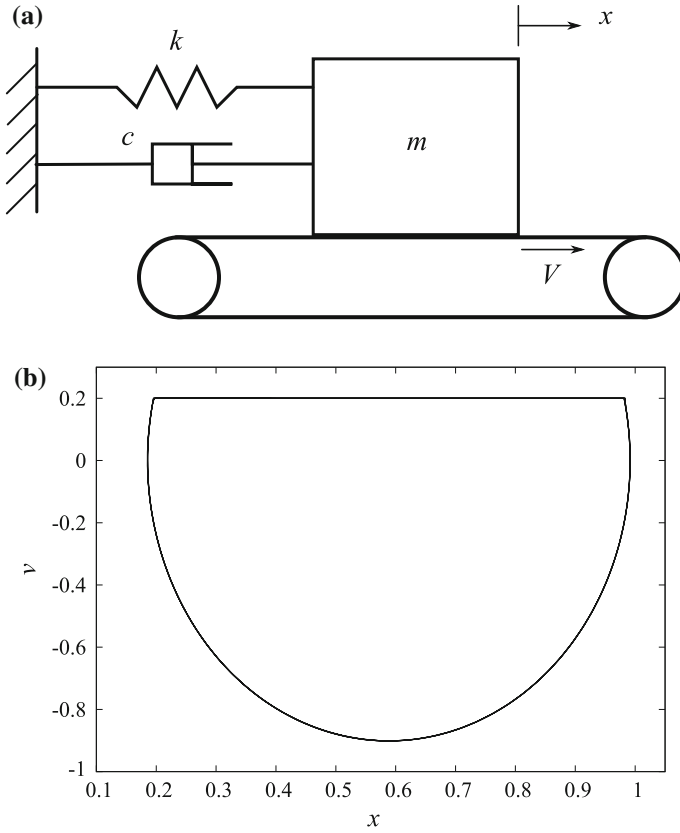


Fig. 2.31 Friction oscillator $m\ddot{x} + c\dot{x} + kx + F_{Coulomb} = 0$, showing **a** a schematic representation of the system, and **b** a phase portrait of a steady-state stick slip oscillation with $m = 2$ kg, $k = 10$ N/m, $F_s = 9.81$ N, $F_d = 5.89$ N, $V = 0.2$ m/s, and $c = 0$

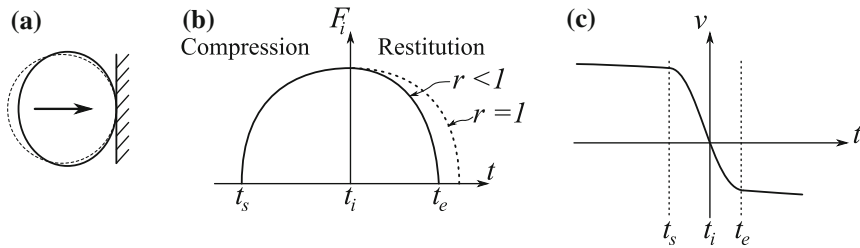


Fig. 2.32 Models for impact, showing **a** a compliant ball impacting a wall, **b** impact force, F_i , against time during impact, and **c** the velocity profile of the ball during impact

where r is the coefficient of restitution, which can be in the range $0 \leq r \leq 1$ with the idealised cases $r = 1$ corresponding to a perfectly elastic impact and $r = 0$ a perfectly plastic impact.

The time of impact starts at time t_s and ends at time t_e . The time at which the impact force, F_i , is a maximum is denoted t_i . For “hard” materials the total time of impact $t_e - t_s$ is relatively small, and r is close to one. In this case it may be justifiable to assume that the time of impact is so small compared to the overall timescales, that the impact can be considered to be instantaneous. This implies that $t_s = t_e = t_i$ and the function in Fig. 2.32b becomes an instantaneous impulse, that can be modelled by a force value multiplied by a Dirac delta function. This in turn leads to a form of the coefficient of restitution law which becomes

$$\dot{x}(t_{i+}) = -r\dot{x}(t_{i-}) \quad (2.34)$$

where t_{i-} is the time immediately before impact and t_{i+} is the time immediately after impact. This simplifies the implementation of the model, as impact time does not have to be computed. However, the model becomes non-smooth and, as was mentioned above for friction models, this can have significant limitations. Several authors have shown examples where this type of instantaneous coefficient model can capture the behaviour of engineering applications, and for an example where the limitations are discussed, see for example Melcher et al. (2013).

Example 2.11 The impact oscillator

Problem The example system shown in Fig. 2.33a consists of a linear, harmonically forced spring-mass-damper system with a motion limiting constraint so that the displacement of the mass, x , is limited to $x \leq d$ and when $x = d$ an impact takes place. A complete model for this system is obtained by combining the equation of motion for a linear harmonically forced oscillator with a coefficient of restitution rule when impact occurs. This system is called an impact oscillator. Using numerical computation find the nonlinear behaviour of this oscillator close to the first natural frequency of the linear oscillator, when $m = 1$ kg, $k = 1$ N/m, $F = 0.5$ N, $c = 0.05$ Ns/m, $d = 1$ m, and Ω is varied between 0 and 2 rad/s.

Solution We can understand the behaviour of this impact oscillator close to the first natural frequency of the linear oscillator by computing a bifurcation diagram. The resulting bifurcation diagram is shown in Fig. 2.33b as the forcing frequency, Ω , is varied. When the displacement amplitude measure $x_{\max-\min}$ is less than d the behaviour is that of a linear oscillator, and it can be seen that the bottom of a resonance curve is visible. However at $x_{\max-\min} = d$ impacts start to occur and complex behaviour such as chaotic motion and multi-period responses can be observed. Overall the resonant peak is hardening, and a region of hysteresis is evident for $\Omega > 1$.

Several alternatives to coefficient of restitution models exist, the most widely used for engineering applications being the Hertzian law of impact. This can be derived by considering the continuum mechanics close to the point of contact, see Stronge (2000) for details. This model is particularly useful for cases when the time of contact and impact force are important to the overall modelling process, but will not be considered further here.

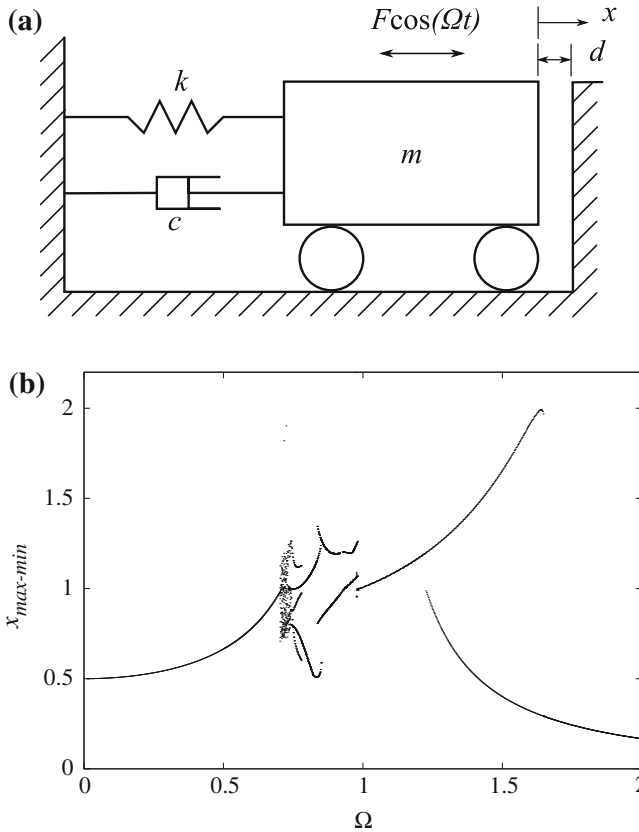


Fig. 2.33 Impact oscillator $m\ddot{x} + c\dot{x} + kx = F\cos(\Omega t)$, for $x < d$ and $\dot{x}(t_{i+}) = -r\dot{x}(t_{i-})$ at $x = d$, showing **a** a schematic representation of the system, and **b** a bifurcation diagram of stable response solutions with $m = 1$ kg, $k = 1$ N/m, $F = 0.5$ N, $c = 0.05$ N s/m, $d = 1$ m, and Ω is varied between 0 and 2 rad/s. Note that $x_{\max-\min}$ is the maximum minus minimum (or peak to peak) x value per forcing period divided by 2

2.8 Nonlinear Phenomena in Higher Dimensions

So far in this chapter the nonlinear phenomena discussed are those which occur in second-order oscillators such as the escape equation or Duffing oscillator. From a vibrations perspective, second-order oscillators are used to model single-degree-of-freedom systems, so what happens when there are multiple degrees-of-freedom?

Some characteristics appear to be similar to linear systems. For example, in a multi-degree-of-freedom nonlinear system there can be multiple resonance peaks, just as in linear systems. However, the resonance peaks will typically be distorted in some way, as in Fig. 2.28. As one would expect, each of these resonance peaks can potentially be excited by an external forcing input. However, unlike for linear systems, in nonlinear multi-degree-of-freedom systems it is possible for *internal resonances*

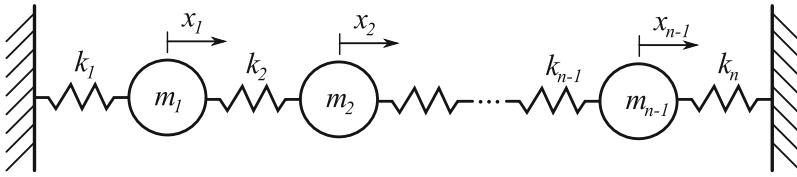


Fig. 2.34 Nonlinear resonance with hysteresis (Duffing)

to occur. This happens when one resonance in the nonlinear system excites another resonance due to coupling between them. Nonlinear systems can also be excited (or forced) by oscillations in the system parameters, so-called *parametric excitation*. When parametric excitation occurs in systems of coupled nonlinear oscillators, resonant behaviour can occur, that may also include internal resonances, sometimes referred to as *auto-parametric excitation*.

2.8.1 The Fermi-Pasta-Ulam Paradox

One of the earliest attempts to understand the dynamics of multi-degree-of freedom nonlinear systems took place in the early 1950s when a group of researchers working at Los Alamos led by Enrico Fermi decided to study the problem of molecular dynamics. The problem they studied looked schematically like that shown in Fig. 2.34, which consists of a chain of masses coupled by nonlinear springs used to represent the interaction of molecules (or atoms) in a solid material. It had already been well established that for a multi-degree-of freedom linear (undamped, unforced) system, energy put into a single mode would remain in that mode for all time. Fermi with his co-workers, Pasta, and Ulam thought that if they put energy into the lowest mode, the nonlinear coupling from the springs would cause the energy to gradually redistribute (or equipartition) into all the modes as time increased. This did happen, however, they also found that if the simulation was run for long enough, the energy flowed back out of all the other modes into the mode where it started. This phenomena was called the Fermi-Pasta-Ulam (FPU) paradox, and gave rise to a large field of research, particularly for Hamiltonian dynamical systems.

Attempts to solve the FPU paradox established important phenomena for nonlinear dynamical systems with multiple degrees-of-freedom. For example the existence of solitary waves or *solitons*, not quite periodic motion otherwise known as *quasi-periodic* motion, and chaos. Another important feature was the interaction of nonlinear resonances, which will be discussed in more depth for vibration problems in Chap. 5.

2.8.2 Localization

Another phenomena that was first established in solid state physics is that of localization. In particular the idea that disorder (or irregularities) in a lattice like structure leads to the confinement of vibrational energy to one localized part of the structure. This phenomena also occurs in structural dynamics and is sometimes referred to as *periodic structure theory*.⁴⁵ An example is shown in Fig. 2.35a, where two pendula are coupled by a linear spring. The length of the pendulum attached to mass m_2 can be varied by a small amount Δl . When the spring stiffness, k , is small and therefore provides only a *weak* coupling between the two masses, localization phenomena can occur. This can be observed by considering the effect of changing Δl on the *linearised* natural frequencies of the system (i.e. assuming small angles). The result of such an investigation is shown in Fig. 2.35b. This shows how the two natural frequency values appear to veer away from each other as they pass through $\Delta l = 0$. This phenomena is known as *mode veering*. It can also be seen that when $\Delta l = 0$ the two natural frequencies are almost identical in value. However, at $\Delta l = 0$ the usual normal modes (equal amplitude in-phase and out-of-phase responses) exist as would be expected for a symmetric two degree-of-freedom linear system. This changes significantly as Δl is increased or decreased, leading to nearly all the energy being confined, or localized, in the vibration of one or other of the pendula.

Note that the natural frequencies veer rather than cross. This is because there is not a multiple eigenvalue for this system at $\Delta l = 0$.

2.8.3 Modelling Approaches

Figure 2.36 shows what can be thought of as a structural dynamics “landscape”. The vertical axis represents the severity of the nonlinearity, from linear at the origin to harsh nonlinearities such as impact and friction in the upper ranges. The horizontal axis represents geometrical complexity, from single-degree-of-freedom oscillators at the origin to millions of degrees-of-freedom (or discretisation points) at the upper end. There are other factors which are not included in this simplified “landscape”, for example the type of external excitation which the system is subjected to. Despite this, the vast majority of nonlinear structural dynamics applications could be plotted at specific points, or regions, in the landscape.

The harmonically forced linear oscillator that was described in Sect. 2.1 is at the origin of Fig. 2.36. All the systems described in Sects. 2.1–2.7, lie on the vertical axis. In Chaps. 4–8 classical structural elements such as beams, cables and plates will be considered. These structures have many degrees-of-freedom and nonlinearity conditions from weak to harsh, and therefore lie away from the axes in Fig. 2.36. That said, analytical techniques such as those described in Chaps. 4–8 are only typically used for relatively small numbers of degrees-of-freedom, typically up to 20.

⁴⁵ See Hodges and Woodhouse (1983) for more details.

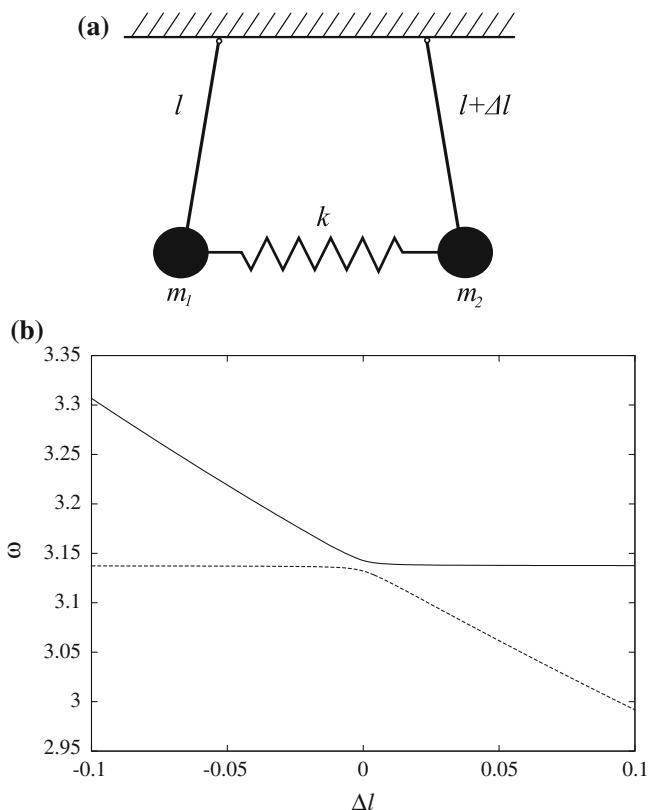


Fig. 2.35 Coupled pendulum system, showing **a** a schematic of the system, and **b** the two natural frequencies of the linearised system as Δl is varied. Parameter values, $m_1 = m_2 = 3$ kg, $l = 1$ m and $k = 0.1$ N/m

But many other systems have complex geometry and/or many degrees of freedom so how can they be modelled? In this case, for structural dynamics, finite element analysis (FEA) is a very powerful tool for creating a model of a system with complex geometry,⁴⁶ see for example Crisfield (1997). However, there is a trade off between representing the complexity of the geometry and understanding the effect of the nonlinearity. This is because creating a model that captures the complexities of the geometry is both computationally expensive and restricts the dynamic analysis which can subsequently be carried out. In fact, most nonlinear phenomena have only really been thoroughly studied and understood for systems with simple geometry, primarily single degree-of-freedom systems.

As a result the part of the landscape in Fig. 2.36 where there is a good understanding of the dynamic behaviour is on the axes and close to the origin. This region is

⁴⁶ This is assuming that the frequencies of interest are in the low range. For mid-frequency problem statistical energy analysis is often more appropriate, see Langley (1989).

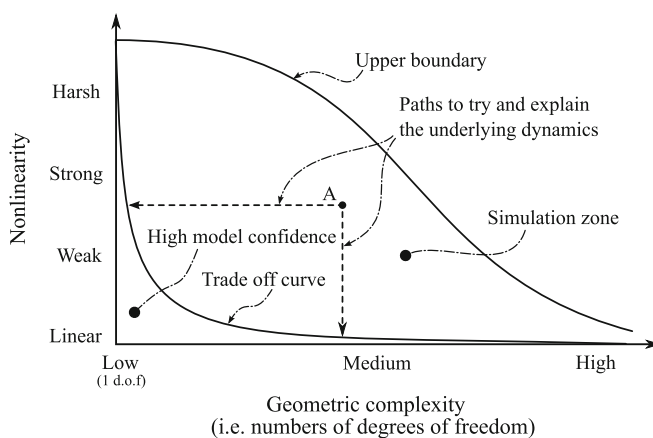


Fig. 2.36 A nonlinear structural dynamics landscape

where high confidence in a model can be achieved.⁴⁷ This is because (i) there is a thorough understanding of the underlying physical behaviour, so that a model can be constructed based on understanding the underlying physics and (ii) the model can typically be validated against experimental or in service data. Beyond this high confidence region, numerical simulations can be used to provide information on the potential behaviour of systems that have combined nonlinearity and complex geometry. However, moving further into this region will typically reduce confidence levels significantly. The upper boundary shown in Fig. 2.36 is set by the available computational power (or cost of computation) and also the confidence in physical models such as impact and friction.

One of the major challenges in structural dynamics is to improve the modelling capability of the simulation zone shown in Fig. 2.36. This is because the ability to carry out a simulation doesn't imply a clear understanding of the simulation results. For example, consider a structure at point A, that has strong nonlinearity and medium geometric complexity, say 1,000 degrees-of-freedom. To try and explain the results of a time-stepping simulation for this system, the choices are to either talk in terms of linear modal systems which exist on the horizontal axis, or strongly nonlinear single degree-of-freedom systems. In other words to project the problem to where understanding and model confidence are greatest. This topic will be discussed further in Chaps. 5 and 6.

2.9 Chapter Notes

This chapter gives an introduction to the nonlinear phenomena observed in vibrating systems. An in-depth treatment of dynamical systems theory is given by Guckenheimer and Holmes (1983), Moon (1987), Cartmell (1990), Glendinning

⁴⁷ Assuming that the modelling techniques employed are used with sufficient care.

(1994), Jordan and Smith (1999), Strogatz (2001) and Thompson and Stewart (2002). Note that Strogatz (2001) offers a particularly good introduction for those who are unfamiliar with the subject. More detailed mathematical treatments of bifurcations can be found in Guckenheimer and Holmes (1983) and Glendinning (1994). A very good treatment of stability via eigenvalue analysis is given by Seyranian and Mailybaev (2003). Relevant aspects of linear vibration theory can be found in Inman (2006). The numerical techniques required can be found in Fausett (1999) for general Matlab and time-integration information and see also Newland (1993), Press et al. (1994) for additional discussions on frequency domain transformations. For an overview of computing mappings and bifurcation diagrams, an excellent paper is by Foale and Thompson (1991). The technique of cell-to-cell mapping is described by Hsu (1987). The delay in actuator example is from Bursi and Wagg (2008), Chap. 7. Mathematical analysis of bifurcation theory is given by Kuznetsov (2004) and Guckenheimer and Holmes (1983), while numerical aspects are discussed by Krauskopf et al. (2007). Topics relating to buckling can be found in Frish-Fay (1962), Thompson and Hunt (1973), Thompson (1982) and Virgin (2000). For topics relating to harsh nonlinearities, friction is covered by Sextro (2002) and Guran et al. (1996), and impact is discussed in depth by Babitsky (1998) and Stronge (2000). Applications of impact oscillator systems can be found in Thompson and Stewart (2002) and a more recent example applied to a flexible beam application is described by Melcher et al. (2013). Detailed treatments of non smooth modelling techniques are given in Brogliato (1999) and di Bernardo et al. (2008). For discussions on the Fermi-Pasta-Ulam problem see Berman and Izrailev (2005) and for localisation see Hodges and Woodhouse (1983) and Pierre (1988) and references therein. Discussion of several multi-degree-of-freedom nonlinear systems are given in Thomsen (2003).

Problems

- 2.1 Derive the equation of motion for the system shown in Fig. 2.20a. Show that this equation can be approximated by the Duffing equation

$$m\ddot{x} + c\dot{x} - \mu x + \alpha x^3 = 0,$$

and estimate when this might be a valid assumption.

- 2.2 The normal form of the Hopf bifurcation is usually written as

$$\begin{aligned}\dot{x} &= \mu x + y - x(x^2 + y^2), \\ \dot{y} &= -x + \mu y - y(x^2 + y^2).\end{aligned}\tag{2.35}$$

Show that this system can also be represented as

$$\begin{aligned}\dot{r} &= r(\mu - r^2), \\ \dot{\theta} &= -1,\end{aligned}$$

in polar coordinates. Examine the stability of the equilibrium point at the origin ($x = 0$, $y = 0$) by finding the Jacobian of Eq. (2.35).

- 2.3 A nonlinear system is governed by the following set of first-order differential equations

$$\begin{aligned}\dot{x}_1 &= x_2, \\ \dot{x}_2 &= x_1 - x_1^2 - \mu x_2,\end{aligned}\tag{2.36}$$

where μ is a parameter which can be varied. Find the equilibrium points for the system when $0 < \mu < \sqrt{4}$ and find the type and stability of each equilibrium point. Sketch typical trajectories in the system state space.

- 2.4 Consider the potential function⁴⁸ given by

$$V = \frac{x_2^2}{2} - \frac{x_1^2}{2} + \frac{x_1^3}{3}.$$

Finding the time derivative of V and substituting for \dot{x}_1 and \dot{x}_2 gives an indication of the stability of equilibrium points at the origin. For the case when x_1 and x_2 are small, use this function to determine the stability of the origin for the system given in Eq. (2.36). How does the sign of \dot{V} relate to the stability?

- 2.5 For the system given in Eq. (2.36), when μ passes through zero a bifurcation occurs. Use local analysis to explain what happens at the bifurcation point. What type of bifurcation occurs?
- 2.6 The dynamics of a damped unforced pendulum can be modelled using the non-linear differential equation

$$\ddot{\theta} + \delta\dot{\theta} + \omega^2 \sin \theta = 0,$$

where θ is the angle of the pendulum from the downwards resting position, δ is the damping parameter and $\omega = \sqrt{\frac{g}{l}}$ is the natural frequency of the pendulum where g is the force due to gravity and l is the length of the pendulum.

Find the equilibrium points for the pendulum in the range $2\pi \leq \theta \leq 2\pi$ when $\delta^2 < 4\omega^2$. Indicate the type and stability of each equilibrium point and sketch the pendulum trajectories in the $\theta, \dot{\theta}$ plane.

- 2.7 For small angles the motion for a pendulum can be approximated by

$$\ddot{\theta} + \delta\dot{\theta} + \omega^2\left(\theta - \frac{\theta^3}{3!}\right) = 0.$$

⁴⁸ Used in this context, this is usually called a Lyapunov function, although limitations exist—see Chap. 3, Sect. 3.2.

Use the potential (i.e. Lyapunov) function

$$V = \frac{1}{2}\dot{\theta}^2 + \frac{\omega^2}{2}\theta^2 - \left(\frac{\omega^2}{3!}\right)\frac{\theta^4}{4}$$

to determine the stability of the point $\theta = 0, \dot{\theta} = 0$, by finding the sign of \dot{V} . Assume that $\omega = 1$.

- 2.8 The logistic map is a single state mapping which is used to model population dynamics represented as

$$x_{n+1} = \lambda x_n(1 - x_n),$$

Identify the period one fixed points for the system and their stability. Which bifurcations occur at $\lambda = 1$ and $\lambda = 3$?

References

- Babitsky, V. I. (1998). *Theory of vibro-impact systems and applications*. Berlin: Springer.
- Berman, G., & Izrailev, F. (2005). The Fermi-Pasta-Ulam problem: Fifty years of progress. *Chaos*, 15(1), 15104.
- Brogliato, B. (1999). *Nonsmooth mechanics: Models, dynamics and control*. London: Springer.
- Bursi, O. S. & Wagg, D. J. (eds.). (2008). *Modern testing techniques for structural systems*. New York: Springer.
- Cartmell, M. (1990). *Introduction to linear, parametric and nonlinear vibrations*. London: Chapman and Hall.
- Crisfield, M. A. (1997). *Non-linear finite element analysis of solids and structures*. In: Advanced Topics (Vol. 2). Chichester: Wiley.
- di Bernardo, M., Budd, C., Champneys, A. R., & Kowalczyk, P. (2008). *Piecewise-smooth dynamical systems: Theory and applications*. London: Springer.
- Diekmann, O., van Gils, S., Verduyn Lunel, S., & Walther, H. (1995). Delay equations. In: Applied mathematical sciences (Vol. 110). New York: Springer.
- Doedel, E. J., Champneys, A. R., Fairgrieve, T. F., Kuznetsov, Y. A., Sandstede, B., & Wang, X. (1998). *Auto97. Continuation and bifurcation software for ordinary differential equations*. Citesteer
- Fausett, L. V. (1999). *Applied numerical analysis using Matlab*. Upper Saddle River, NJ: Prentice Hall.
- Foale, S., & Thompson, J. M. T. (1991). Geometrical concepts and computational techniques of nonlinear dynamics. *Computer Methods for Applications in Mechanical Engineering*, 89, 381–394.
- Frish-Fay, R. (1962). *Flexible bars*. London: Butterworths.
- Glendinning, P. (1994). *Stability, instability and chaos*. Cambridge: Cambridge University Press.
- Guckenheimer, J., & Holmes, P. (1983). *Nonlinear oscillations, dynamical systems, and bifurcations of vector fields*. New York: Springer.
- Guran, A., Pfeiffer, F., & Popp, K. (1996). *Dynamics with friction*. Singapore: World Scientific Publishing.
- Hodges, C. H., & Woodhouse, J. (1983). Vibration isolation from irregularity in a nearly periodic structure—theory and measurements. *Journal of the Acoustical Society of America*, 74(3), 894–905.
- Hsu, C. S. (1987). *Cell-to-cell mapping*. New York: Springer.

- Inman, D. J. (2006). *Vibration with control*. Chichester: Wiley.
- Jordan, D. W., & Smith, P. (1999). *Nonlinear ordinary differential equations; an introduction to dynamical systems* (3rd ed). Oxford: Oxford University Press.
- Krauskopf, B., Osinga, H. M., & Galan-Vioque, J. (eds.). (2007). *Numerical continuation methods for dynamical systems*. New York: Springer.
- Kuznetsov, Y. A. (2004). *Elements of applied bifurcation theory*. New York: Springer.
- Langley, R. S. (1989). A general derivation of the statistical energy analysis equations for coupled dynamic systems. *Journal of Sound and Vibration*, 135(3), 499–508.
- Melcher, J., Champneys, A. R., & Wagg, D. J. (2013). The impacting cantilever: Modal non-convergence and the importance of stiffness matching. *Philosophical Transactions of the Royal Society A: Mathematical, Physical and Engineering Sciences*, 371(1993), 1471–2962.
- McInnes, C. R., Gorman, D. G., & Cartmell, M. P. (2008). Enhanced vibrational energy harvesting using nonlinear stochastic resonance. *Journal of Sound and Vibration*, 318, 655–662.
- Moore, F. C. (1987). *Chaotic vibrations: An introduction for applied scientists and engineers*. New York: Wiley.
- Newland, D. E. (1993). *An introduction to random vibrations and spectral analysis*. Pearson: Prentice Hall.
- Pierre, C. (1988). Mode localization and eigenvalue loci veering phenomena in disordered structures. *Journal of Sound and Vibration*, 126(3), 485–502.
- Press, W. H., Teukolsky, S. A., Vetterling, W. T., & Flannery, B. P. (1994). *Numerical recipes* (2nd ed). Cambridge: Cambridge University Press.
- Sextro, W. (2002). *Dynamical contact problems with friction: Models, methods. Experiments and applications*. New York: Springer.
- Seyranian, A. P., & Mailybaev, A. A. (2003). *Multiparameter stability theory with mechanical applications*. Singapore: World Scientific Publishing.
- Sontag, E. D. (1998). *Mathematical control theory*. New York: Springer.
- Stépan, G. (1989). *Retarded dynamical systems: Stability and characteristic functions*. Essex: Longman Scientific & Technical.
- Strogatz, S. H. (2001). *Nonlinear dynamics and chaos*. Cambridge: Perseus Books Group.
- Stronge, W. J. (2000). *Impact mechanics*. Cambridge: Cambridge University Press.
- Thompson, J. M. T. (1982). *Instabilities and catastrophes in science and engineering*. Chichester: Wiley.
- Thompson, J. M. T., & Hunt, G. W. (1973). *A general theory of elastic stability*. Chichester: Wiley.
- Thompson, J. M. T., & Stewart, H. B. (2002). *Nonlinear dynamics and chaos*. Chichester: Wiley.
- Thomsen, J. J. (2003). *Vibrations and stability: Advanced theory, analysis and tools*. New York: Springer.
- Virgin, L. N. (2000). *An introduction to experimental nonlinear dynamics*. Cambridge: Cambridge University Press.
- Virgin, L. N. (2007). *Vibration of axially-loaded structures*. Cambridge: Cambridge University Press.

<http://www.springer.com/978-3-319-10643-4>

Nonlinear Vibration with Control
For Flexible and Adaptive Structures

Wagg, D.; Neild, S.

2015, XI, 453 p. 142 illus., 3 illus. in color., Hardcover

ISBN: 978-3-319-10643-4